Inorganic Chemistry

Article

pubs.acs.org/IC

A New Family of Ni_4 and Ni_6 Aggregates from the Self-Assembly of $[Ni_2]$ Building Units: Role of Carboxylate and Carbonate Bridges

Moumita Pait,[†] Antonio Bauzá,[‡] Antonio Frontera,[‡] Enrique Colacio,[§] and Debashis Ray*[,†]

[†]Department of Chemistry, Indian Institute of Technology (IIT), Kharagpur 721 302, India

[‡]Departament de Química, Universitat de les Illes Balears (UIB), Carretera de Valldemossa, km 7,5, 07122 Palma, Balearic Islands, Spain

[§]Departamento de Quımica Inorganica, Facultad de Ciencias, Universidad de Granada, 18071 Granada, Spain

Supporting Information

ABSTRACT: Carboxylato (R = ^{t}Bu and Et) and carbonato bridges have been utilized for nickel(II)-based aggregates $[Ni_4(\mu\text{-}H_2L)_2(\mu_3\text{-}OH)_2(\mu_{1,3}\text{-}O_2CBu^t)_2](NO_3)_2\cdot H_2O\cdot 2DMF$ (**1**·H_2O·2DMF), $Ni_4(\mu\text{-}^{hy}HL)_2(\mu_3\text{-}OMe)_2(\mu_{1,1}\text{-}N_3)_2(\mu_{1,3}\text{-}O_2CEt)_2]\cdot 4H_2O$ (**2**·4H_2O), and $Ni_6(\mu_4\text{-}L)(\mu_3\text{-}L)_2(\mu_6\text{-}CO_3)(H_2O)_8](ClO_4)\cdot 9H_2O$ (**3**·9H_2O). Building blocks $[Ni_2(\mu\text{-}H_2L)]^{3+}$, $[Ni_2(\mu\text{-}^{hy}HL)]^{3+}$, and $[Ni_2(\mu\text{-}L)]^{+}$ originating from $[Ni_2(\mu\text{-}H_2L)]^{3+}$ have been trapped in these complexes. The complexes have been characterized by X-ray crystallography, magnetic measurements, and density functional theory (DFT) analysis. In **1**, the magnetic interactions are transmitted through the μ_3-phenoxido/μ_3-hydroxido/*syn*−*syn*-^{t}BuCO$_2^-$, μ_3-phenoxido/μ_3- hydroxido, and double μ_3-phenoxido/double μ_3-hydroxido bridges with J = +11.4 cm^{-1}, J_1 = −2.1 cm^{-1}, and J_2 = −2.8 cm^{-1}, respectively. In **2**, the interactions are ferromagnetic, with J_1 = +27.5 cm^{-1}, J_2 = +20.62 cm^{-1}, and J_3 = +1.52 cm^{-1} describing the magnetic couplings through the μ-phenoxidoo/μ_3-methoxido, μ-azido/μ_3-methoxido, and μ_3-methoxido/μ_3-methoxido exchange pathways, respectively. Complex **3** gives J_1 = −3.30 cm^{-1}, J_2 = +1.7 cm^{-1}, and J_3 = −12.8 cm^{-1} for exchange pathways mediated by μ-phenoxido/μ-carbonato, μ-alkoxido/μ-alkooxido/μ-*syn*−*syn*-carbonato, and the μ-phenoxido/μ-carbonato, respectively. Interestingly, **1** and **3** below 20 K and 35 K, respectively, show an abrupt increase of the $\chi_M T$ product to reach a magnetic-field-dependent maximum, which is associated with a slightly frequency-dependent out-of-phase alternating-current peak. DFT calculations have also been performed on **1**−**3** to explain the exchange interaction mechanisms and to support the magnitude and sign of the magnetic coupling constants between the Ni^{II} ions.

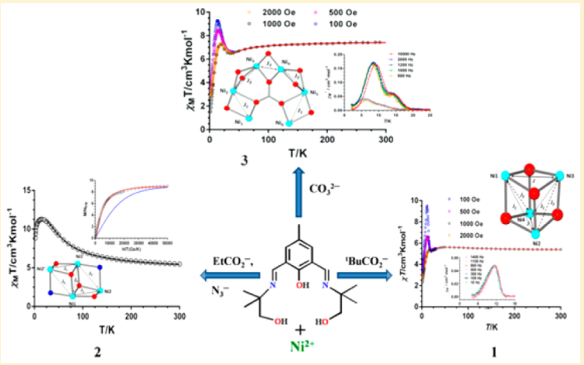

INTRODUCTION

The synthetic multinuclear coordination chemistry of 3d metal ions based on guided and controlled aggregation via the self-assembly of mono- or dinuclear building units has become of contemporary interest because of their relevance from bioinorganic chemistry to new magnetic materials.[1] The roles of phenoxido donors in bridging two or more metal ions and in fine-tuning reaction conditions with added and in situ generated ancillary ligands are decisive to understanding and controling the varying structures obtained through self-aggregation processes. Solution-based room temperature synthesis of tetranuclearity and other higher nuclearity nickel complexes has become a promising class of aggregative coordination complexes in which variation of the metal salt, coordinating ligand, ancillary groups, and added bases leads to a variety of structural motifs showing characteristic magnetic properties.[2] The guiding factor for the coordination aggregate formation is "spontaneous self-assembly", in which all of the components are simply mixed in solution with magnetic stirring at room temperature and the powdered sample thus obtained is left to crystallize. Several of these self-aggregates based on the Ni^{II} ion can behave as single-molecule magnets (SMMs) because of the blend of a large ground-state spin (S) with a large magnetic anisotropy that originates from a negative and axial zero-field-splitting (ZFS) parameter (D).[3]

Thus, the demand for new synthetic approaches is there for high-spin multimetallic coordination complexes with promise for SMM behavior.[7,8] The phenol-bearing "dinucleating ligands" able to bind simultaneously two metal ions would be the most promising choice for newer self-aggregation routes using dinuclear building motifs. Bearing two adjacent imine arms, this type of ligand can afford M_2L-type building units.[9] Such a strategy can also offer novel structures and properties in the assembly of transition-metal aggregates from two or more Ni_2L units.[4c,5,6,10,11] Along with the metal-bound ligand unit, small bridges like hydroxide, methoxide, oxide, phenolate, carboxylate, carbonate, azide, etc., can result in the growth of a

Received: January 6, 2015
Published: May 1, 2015

DOI: 10.1021/acs.inorgchem.5b00039
Inorg. Chem. 2015, 54, 4709−4723

variety of topologies, e.g., cubane,[12] fused defective dicubane,[13] pentanuclear vertex-shared open dicubane,[11,14] and hexanuclear chairlike form.[15] With their versatile bridging modes (Scheme S1 in the Supporting Information, SI), the anionic groups also can propagate magnetic interactions between the paramagnetic metal centers. Among various bridging modes of azide, $\mu_{1,1}$-(end-on, EO, c) favors ferromagnetic coupling,[16] whereas $\mu_{1,3}$-(end-to-end, EE, e) transmits antiferromagnetic interactions.[17] Carboxylate groups can adopt numerous coordination modes such as terminal, chelating, and bridging syn−anti in μ-1,1 mode (l), syn−syn, syn−anti, and anti−anti in μ-1,3 mode (m-o), anti−syn−syn and anti−syn−anti in μ_3-1,1,3 mode (p), and syn−anti−syn−anti in μ_4-1,1,3,3 mode (q) (Scheme S1 in the SI), satisfying the coordination requirement and charge demand of the transition-metal ions.[18−20] The syn−syn and anti−anti coordination results in antiferromagnetic interaction, whereas the syn−anti mode mediates either weak ferromagnetic or antiferromagnetic interaction.[21] The carbonate ion can bridge two to six metal ions with its diverse coordination modes (r−w). Among these bridging-*cum*-nucleating modes, r,[22−27] s,[28] and v[29] led to very strong antiferromagnetic behavior for nickel(II) compounds.[22,23,27,28] However, the mode w responsible for trapping six metal ions is less common and shows strong ferromagnetic interactions (Scheme S1 in the SI).[30−32]

In this context, we have been interested in exploring the reactivity of multinucleating Schiff base ligand H_3L (Scheme 1,

Scheme 1. Drawings of Ligands H_3L and $^{hy}H_2L$

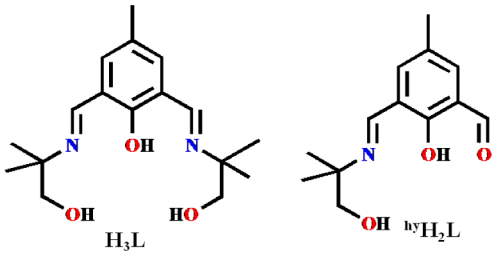

left) and nickel(II) salts in three different reaction conditions. The use of this ligand in transition-metal cluster complexes is relatively new, although some noteworthy results of $[Cu_6]$ have been reported.[33] The aggregating ability of H_3L, together with the cage-forming potential of hydroxide, methoxide, azide, carboxylate, and carbonate, has now been explored here with the preparation of cubane and fused-dicubane cages $[Ni_4(\mu_3\text{-}OH)_2(\mu\text{-}H_2L)_2(\mu_{1,3}\text{-}O_2CBu^t)_2]\cdot(NO_3)_2\cdot H_2O\cdot 2DMF$ ($\mathbf{1}\cdot H_2O\cdot 2DMF$), $[Ni_4(\mu\text{-}^{hy}L)_2(\mu_3\text{-}OMe)_2(\mu_{1,1}\text{-}N_3)_2(\mu_{1,3}\text{-}O_2CEt)_2]\cdot 4H_2O$ ($\mathbf{2}\cdot 4H_2O$), and the novel hexanuclear aggregate $Ni_6(\mu_4\text{-}L)(\mu_3\text{-}L)_2(\mu_6\text{-}CO_3)(H_2O)_8](ClO_4)\cdot 9H_2O$ ($\mathbf{3}\cdot 9H_2O$). The formation of $\mathbf{2}\cdot 4H_2O$ revealed a coordination-driven partial hydrolysis reaction of the parent Schiff base ligand (Scheme S3 in the SI). The used ligand has been proven to be versatile and used to cap the specific faces of the cubane, partial dicubane, and hexanuclear aggregate. Apart from the bridging capacity of the central phenoxido group of the ligand, the aggregating potential of the alcohol side arms of H_3L contributes differently during the formation of three different aggregates, **1**−**3** (Scheme 2).

We were unable to isolate any form of the dinuclear precursor most probably because of the spontaneous self-assembly reactions.

Scheme 2. Observed Ligand-Bonding Modes of H_2L^-, $^{hy}HL^-$, L^{3-}, HO^-, MeO^-, N_3^-, RCO_2^-, and CO_3^{2-}

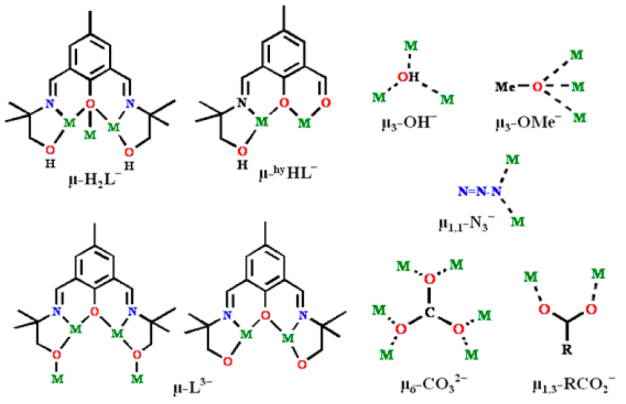

EXPERIMENTAL SECTION

Materials. The solvents and chemicals used were obtained from commercial sources like SRL, India, Sigma-Aldrich, and Loba Chemie Laboratory Reagents & Fine Chemicals, India. Nickel perchlorate hexahydrate was freshly prepared by treating nickel carbonate (11.8 g, 0.1 mol) with 12.03 mL of perchloric acid (1:2) and crystallized after concentration on a water bath. Sodium salts of pivalic acid and propanoic acid are prepared by treating pivalic acid (15.3 g, 0.15 mol) and propanoic acid (11.22 g, 0.15 mol) with solid sodium hydroxide (6.0 g, 0.15 mol), followed by concentration and crystallization on a water bath. All other chemicals and solvents were reagent-grade materials and were used as received without further purification.

Caution! *Azide and perchlorate salts of metal ions involving organic ligands are potentially explosive. Only small quantities of the complexes should be prepared, and these should be handled with proper care.*

Synthesis. H_3L Ligand. The ligand 2,6-bis[[2-hydroxy-(1,1-dimethylethyl)imino]methyl]-4-methylphenol used in the present work is prepared from the single-step condensation of 2,6-diformyl-4-methylphenol (0.328 g, 2 mmol) and 2-amino-2-methyl-1-propanol (0.381 g, 4 mmol) in methanol (MeOH; 25 mL) under reflux for 1 h, followed by solvent evaporation to get a gummy mass as reported previously.[33] The ligand is washed with toluene, and recrystallization from ethyl acetate yields orange crystals of the ligand (Scheme S2 in the SI).

$[Ni_4(\mu_3\text{-}OH)_2(H_2L)_2(\mu_{1,3}\text{-}O_2CBu^t)_2](NO_3)_2\cdot H_2O\cdot 2DMF$ ($\mathbf{1}\cdot H_2O\cdot 2DMF$). To the yellow MeOH solution (20 mL) of H_3L (0.306 g, 1.00 mmol) is added slowly a MeOH solution (10 mL) of $Ni(NO_3)_2\cdot 6H_2O$ (0.580 g, 2.00 mmol), followed by the dropwise addition of NEt_3 (0.558 g, 4 mmol) with stirring at room temperature in air. The brown solution formed initially changes to green during complete addition of NEt_3. The resulting green solution is stirred for ca. 30 min, and an aqueous solution of $^tBuCO_2Na$ (0.123 g, 1 mmol) is added dropwise to the reaction mixture. The stirring is continued for another 30 min. The solvent is evaporated in air to give a green solid, which is isolated by filtration, washed with cold MeOH, and dried under vacuum over P_4O_{10}. The green plate-shaped single crystals suitable for X-ray analysis are obtained from a *N*,*N*-dimethylformamide (DMF) solution of the powdered solid after 1 month. Yield: 0.442 g, 64.5%. Anal. Calcd for $C_{50}H_{88}N_8Ni_4O_{21}$ (1374.06 g mol^{-1}): C, 43.71; H, 6.60; N, 8.15. Found: C, 42.90; H, 6.50; N, 8.22. Selected FT-IR bands (KBr, cm^{-1}; s = strong, vs = very strong, m = medium, br = broad): 3485 (br), 1652 (s), 1567 (vs), 1388 (m), 1384 (vs). Molar conductance, Λ_M (DMF solution): 149 S m^2 mol^{-1}. UV−vis spectra [λ_{max}, nm (ε, L mol^{-1} cm^{-1}); MeOH solution]: 663 (120), 372 (8184), 254 (39273).

$[Ni_4(\mu\text{-}^{hy}HL)_2(\mu_3\text{-}OMe)_2(\mu_{1,1}\text{-}N_3)_2(\mu_{1,3}\text{-}O_2CEt)_2]\cdot 4H_2O$ ($\mathbf{2}\cdot 4H_2O$). To a green solution of $Ni(NO_3)_2\cdot 6H_2O$ (0.580 g, 2.00 mmol) in MeOH (20 mL) is added another MeOH solution of H_3L (0.306 g, 1 mmol), and the resulting solution is stirred for 15 min, during which time an aqueous solution of $EtCO_2Na$ (0.096 g, 1 mmol) is added dropwise. The light-green solution is stirred for 5 min, and then an aqueous

DOI: 10.1021/acs.inorgchem.5b00039
Inorg. Chem. 2015, 54, 4709−4723

solution of NaN_3 (0.065 g, 1 mmol) is slowly added in small portions, resulting in the formation of a dark-green solution. This is stirred for a further 30 min and filtered, and the filtrate is allowed to stand undisturbed at room temperature. After about 1 week, green needle-shaped crystals suitable for X-ray study are obtained. Yield: 0.212 g, 40%. Anal. Calcd for $C_{34}H_{46}N_8Ni_4O_{14}$ (1062.11 g mol^{-1}): C, 39.82; H, 4.52; N, 10.93. Found: C, 39.86; H, 5.19; N, 10.83. Selected FT-IR bands: 3464 (br), 2066 (s), 1649 (s), 1559 (s), 1458 (m), 1406 (m), 1044 (m). Molar conductance, Λ_M (MeOH solution): 21 S m^2 mol^{-1}. UV–vis spectra [λ_{max}, nm (ε, L mol^{-1} cm^{-1}); MeOH solution]: 674 (400), 405 (9743), 246 (27613).

*[$Ni_6(\mu_4$-L)$(\mu_3$-L)$_2(\mu_6$-$CO_3)(H_2O)_8](ClO_4)\cdot 9H_2O$ (**3**$\cdot 9H_2O$). Method A via CO_2 Fixation.* A MeOH solution (10 mL) of H_3L (0.306 g, 1 mmol) is added to an aqueous solution of NaOH (0.04 g, 1 mmol), and the mixture is stirred for 30 min. The addition of a solution of $Ni(ClO_4)_2\cdot 6H_2O$ (0.73 g, 2 mmol) in MeOH (15 mL) to the previous solution resulted in a change of solution color from light to dark green during 1 h stirring of the reaction mixture at laboratory temperature. The solution is next filtered through a G4 sintered-glass bed and allowed to evaporate slowly for supersaturation. After 7 days, green single crystals of **3**$\cdot 9H_2O$ suitable for X-ray diffraction are isolated. Yield: 0.159 g, 27.8%. Anal. Calcd for $C_{53}H_{69}ClN_6Ni_6O_{33}$ (1711.88 g mol^{-1}): C, 36.48; H, 5.12; N, 4.91. Found: C, 36.73; H, 5.32; N, 5.01. Selected FT-IR bands: 3429 (br), 1639 (s), 1449 (m), 1058 (m), 836 (m), 622 (m). Molar conductance, Λ_M (MeOH solution): 94 S m^2 mol^{-1}. UV–vis spectra [λ_{max}, nm (ε, L mol^{-1} cm^{-1}); MeOH solution]: 673 (415), 400 (2389), 258 (61561).

Method B Using Carbonate Salt. Solid K_2CO_3 (0.27 g, 2 mmol) is added to a stirred MeOH solution of H_3L (0.306 g, 1 mmol), and stirring is continued for 2 h. To this yellow solution is added a MeOH solution (10 mL) of $Ni(ClO_4)_2\cdot 6H_2O$ (0.73 g, 2 mmol), and the resulting solution is stirred for 1 h to get a dark-green solution. The solution is then filtered and kept for crystallization. After 1 week, the obtained crystals are collected, washed with a small amount of MeOH, and dried under vacuum. Yield: 0.398 g, 69.7%.

Physical Measurements. Elemental analyses (C, H, and N) were performed with a PerkinElmer model 240C elemental analyzer. FT-IR spectra were recorded on a PerkinElmer 883 spectrometer. The solution electrical conductivity and electronic spectra were obtained using a Unitech type U131C digital conductivity meter with a solute concentration of about 10^{-3} M and a Shimadzu UV 3100 UV–vis–near-IR spectrophotometer, respectively. The purity of powder complexes for all three samples was determined by PXRD using a Bruker AXS X-ray diffractrometer (40 kV, 20 mA) using Cu Kα radiation (λ = 1.5418 Å) over the 5–50° (2θ) angular range and a fixed-time counting of 4 s at 25 °C. Variable-temperature magnetic susceptibility and magnetization measurements were carried out with a Quantum Design SQUID MPMS XL5 magnetometer on polycrystalline samples of complexes **1**–**3** under an applied field of 1000 Oe. Alternating-current (ac) susceptibility measurements under different applied static fields were performed using an oscillating ac field of 3.5 Oe and ac frequencies ranging from 1 to 1500 Hz. The experimental susceptibilities were corrected for the sample holder and diamagnetism of the constituent atoms by using Pascal's constants.

Theoretical Methods. Calculations have been carried out using density functional theory (DFT) combined with the broken-symmetry approach[34,35] by means of the *Gaussian 09* package.[36] The level of theory used in this study is B3LYP/6-31+G*, which is a good compromise between the size of the system and the computational demands. For these calculations, we have used the crystallographic coordinates. It should be mentioned that the widely and successfully used[37−39] broken-symmetry DFT approach is not a unique methodology to compute and interpret the magnetic properties in quantum chemistry. For instance, ab initio methods based on difference dedicated configuration interaction[40] (e.g., CASSCF/DDCI) give excellent results and offer the possibility to finely analyze the mechanisms and origin of the magnetic properties, taking advantage of access to the wave function of all spin states of interest. However, this methodology was not used for systems studied herein for computational reasons because some complexes have more than 100 atoms.

X-ray Crystallography. X-ray diffraction data on suitable single crystals of **1**$\cdot H_2O\cdot$2DMF, **2**$\cdot 4H_2O$, and **3**$\cdot 9H_2O$ were collected using a Bruker SMART APEX-II CCD diffractometer, equipped with a fine-focus 1.75 kW sealed tube with Mo Kα radiation (λ) 0.71073 Å at 298 K, with increasing ω (width of 0.3° frame^{-1}) at a scan speed of 5 s frame^{-1}. *SMART* software was used for data acquisition. Space group determination and data integration and reduction were performed with *XPREP* and *SAINT* software.[41] Structures were solved by direct methods using *SHELXS-97*[42a] and refined with full-matrix least squares on F^2 using the *SHELXL-97*[42b] program package. All non-H atoms were refined anisotropically. Multiscan empirical absorption corrections were applied to the data using the program *SADABS*.[43] The locations of the heaviest atoms (Ni) were easily determined, and the O, N, and C atoms were subsequently determined from the difference Fourier maps. The non-H atoms were refined anisotropicly (except O59 in complex **3**). The H atoms were introduced in calculated positions and refined with fixed geometry with respect to their carrier atoms. A summary of the crystal data and relevant refinement parameters is given in Table 1. CCDC 922994 (**1**), 922993 (**2**), and 922995 (**3**) are given as crystallographic data in the SI. These data can also be obtained free of charge at www.ccdc.cam.ac.uk/conts/retrieving.html (or from the Cambridge Crystallographic Data Centre,

Table 1. Crystal Parameters and Refinement Data for 1$\cdot H_2O\cdot$2DMF, 2$\cdot 4H_2O$, and 3$\cdot 9H_2O$

	1$\cdot H_2O\cdot$2DMF	**2**$\cdot 4H_2O$	**3**$\cdot 9H_2O$
empirical formula	$C_{50}H_{90}N_8Ni_4O_{21}$	$C_{34}H_{54}N_8Ni_4O_{16}$	$C_{52}H_{87}ClN_6Ni_6O_{33}$
fw (g mol^{-1})	1374.06	1062.11	1711.88
cryst syst	triclinic	triclinic	monoclinic
space group	$P\bar{1}$	$P\bar{1}$	$P21/c$
cryst color	green	green	green
cryst dimens (mm^3)	0.32 × 0.27 × 0.22	0.34 × 0.29 × 0.25	0.33 × 0.29 × 0.24
a (Å)	11.2454(16)	9.522(2)	16.9227(6)
b (Å)	14.308(2)	14.168(3)	24.5016(8)
c (Å)	21.196(3)	17.741(4)	23.0290(7)
α (deg)	77.757(4)	91.600(7)	90.00
β (deg)	81.451(4)	102.804(7)	127.462(2)
γ (deg)	75.416(4)	94.272(6)	90.00
V (Å)	3209.1(8)	2324.9(8)	7579.3(4)
Z	2	2	4
T (K)	298(2)	298(2)	298(2)
μ (mm^{-1})	1.231	1.668	1.580
ρ_{calcd} (Mg m^{-3})	1.420	1.528	1.500
F(000)	1448	1104	3488
no.of reflns collected	41706	31446	73696
no. of unique reflns	12938	11235	12508
no. of param	768	559	893
R1[a] [$I > 2\sigma(I)$]	0.0560	0.0744	0.0557
wR2[b] (all data)	0.1541	0.2465	0.1667
R(int)	0.0664	0.0641	0.0713
GOF (F^2)	1.044	1.013	1.024
largest diff peak and hole (e $Å^{-3}$)	0.593 and −0.623	0.949 and −0.804	1.660 and −0.525
CCDC no.	922994	922993	922995

[a]R1 = $\sum(||F_o| - |F_c||)/\sum|F_o|$. [b]wR2 = $[\sum w(|F_o| - |F_c|)^2/\sum w(F_o)^2]^{1/2}$, where $w = 0.75/[\sigma^2(F_o) + 0.0010F_o^2]$.

DOI: 10.1021/acs.inorgchem.5b00039
Inorg. Chem. 2015, 54, 4709−4723

12 Union Road, Cambridge CB2 1EZ, U.K.; fax +44-1223/336-033; e-mail deposit@ccdc.cam.ac.uk).

RESULTS AND DISCUSSION

Synthetic Considerations. The phenol-bearing ligand 2,6-bis-[[2-hydroxy-(1,1-dimethylethyl)imino]methyl]-4-methylphenol (H_3L) has been synthesized via a standard Schiff base condensation reaction (Scheme S2 in the SI) following a literature procedure,[33] and its reactions with nickel(II) salts have been methodically explored to obtain a new family of coordination aggregates (Scheme S4 in the SI). The reaction of $Ni(NO_3)_2{\cdot}6H_2O$ with H_3L and $^tBuCO_2Na$ in MeOH and in the presence of base NEt_3 in 2:1:2 stoichiometry led to the formation of compound **1** as a green powder from the reaction mixture in 64% yield. The synthesis of **1** can be summarized by eq 1:

$$4Ni(NO_3)_2{\cdot}6H_2O + 2H_3L + 4{}^tBuCO_2Na + 4NEt_3 \xrightarrow{DMF} [Ni_4(H_2L)_2(OH)_2({}^tBuCO_2)_2](NO_3)_2 \cdot 2DMF + 4(NHEt_3)NO_3 + 2NaNO_3 + 21H_2O \ldots \quad (1)$$

Room temperature evaporation of a DMF solution of **1** gave a suitable crystal of $\mathbf{1}{\cdot}H_2O{\cdot}2DMF$ for X-ray structure determination. The elemental analysis and molar conductivity data are consistent with the composition $[Ni_4(H_2L)_2(OH)_2({}^tBuCO_2)_2](NO_3)_2{\cdot}H_2O{\cdot}2DMF$. The use of $Ni(ClO_4)_2{\cdot}6H_2O$ or $NiCl_2{\cdot}6H_2O$ in place of $Ni(NO_3)_2{\cdot}6H_2O$ results in a green gummy mass not suitable for thorough physical characterization. Interestingly, when sodium propanoate is used in place of sodium pivalate along with sodium azide (2:1:1:1 molar ratio) in a reaction protocol similar to that of eq 1 in MeOH, complex **2** is obtained. The synthesis of **2** can be summarized by eq 2:

$$4Ni(NO_3)_2{\cdot}6H_2O + 2H_3L + 2NaN_3 + 4EtCO_2Na \xrightarrow{MeOH} [Ni_4({}^{hy}HL)_2(OMe)_2(N_3)_2(EtCO_2)_2]{\cdot}4H_2O + 2EtCO_2H + 2[NH_3C(Me)_2CH_2OH]NO_3 + 6NaNO_3 + 20H_2O \ldots \quad (2)$$

In this reaction condition, the parent ligand H_3L undergoes single imine arm hydrolysis in the presence of metal ions to provide $^{hy}H_2L$.[44,45] Green needlelike single crystals of $\mathbf{2}{\cdot}4H_2O$ were obtained from room temperature slow evaporation of the reaction mixture. Establishment of the composition of $\mathbf{2}{\cdot}4H_2O$ as $[Ni_4({}^{hy}HL)_2(OMe)_2(N_3)_2(EtCO_2)_2]{\cdot}4H_2O$ is done from standard elemental analysis and molar conductivity studies. The reaction with an excess amount of azide anion did not lead to the substitution of methoxido bridges in $\mathbf{2}{\cdot}4H_2O$, indicating the strong affinity and stability of two MeO^- supports in this system. Next we carried out another reaction in a strong alkaline medium by using NaOH as the base. The reaction of H_3L with a double molar amount of $Ni(ClO_4)_2$ in the presence of a strong base (NaOMe or NaOH) in MeOH leads to crystals of $\mathbf{3}{\cdot}9H_2O$ in relatively low yield (27%) following CO_2 uptake from the atmosphere, according to eq 3:

$$6Ni(ClO_4)_2{\cdot}6H_2O + 3H_3L + 11NaOH + CO_2 \rightarrow [Ni_6(L)_3(CO_3)(H_2O)_8]ClO_4{\cdot}9H_2O + 11NaClO_4 + 29H_2O \ldots \quad (3)$$

This also indicates that the formation of $\mathbf{3}{\cdot}9H_2O$ constitutes a significant driving force toward the capture of CO_2 from the atmosphere in the basic conditions. In the presence of a strong base, in situ generation of a single carbonate ligand is responsible for the self-assembly of three dinuclear fragments for the formation of a novel $[Ni_6O_6]$ cluster. Bases like NEt_3 and NaN_3 did not facilitate the trapping of CO_2 from the atmosphere. On the other hand, CO_3^{2-} may be added in the form of a metallic salt to the reaction mixture, which also leads to the generation of complex $\mathbf{3}{\cdot}9H_2O$. Thus, the addition of $Ni(ClO_4)_2{\cdot}6H_2O$ to a stirred MeOH solution of H_3L and K_2CO_3 leads to the formation of a hexanuclear aggregate (as described in eq 4) at high yield (69%) compared to the previous procedure.

$$6Ni(ClO_4)_2{\cdot}6H_2O + 3H_3L + 6K_2CO_3 \rightarrow [Ni_6(L)_3(CO_3)(H_2O)_8]ClO_4{\cdot}9H_2O + 11KClO_4 + KOH + 5CO_2 + 23H_2O \ldots \quad (4)$$

Elemental analysis and molar conductivity data agree with the formula for **3** as given above and further confirmed by molecular structure determination.

Roles of Carboxylato and Carbonato Ancillary Ligands for Different Molecular Self-Assemblies. Subtle changes in the reaction conditions deliver three different types of aggregation reactions for the self-assembly of ligated dinuclear nickel(II) building units. In the reported reaction conditions, $\mu_{1,3}$-bridging modes of $^tBuCO_2^-$ and $EtCO_2^-$ groups play the decisive role in trapping the solvent-derived HO^- and MeO^- selectively within tetranuclear nickel(II) cubane and open-dicubane assemblies in **1** and **2**. The use of $^tBuCO_2^-$ could not trap MeO^- for a cube structure similar to **1** and $EtCO_2^-$ for the entrapment of HO^- for an open-dicubane structure like **2**. The R groups attached to the carboxylate functions thus can modulate the metal−ligand aggregation routes from the pool of small ancillary linkers of varying bridging potential. Thus, two different carboxylate-group-bound $[Ni_2]$ motifs self-assemble in two different ways to produce **1** and **2**. The carbonate ion encapsulated within complex **3** is presumably derived from the fixation of atmospheric CO_2 and has attracted renewable interest in this area because of the formation of a clusterlike coordination complex. Fixation of atmospheric CO_2 did not lead to any HCO_3^- for carboxylate-like bridging to provide either a cube or an open-dicubane molecular assembly. In the presence of carboxylates and carbonates, the parent ligand system H_3L showed different levels of deprotonation, hydrolysis, and coordination. In all three cases, carboxylato and carbonato bridges support the phenoxido bridges in hitherto nonisolable dinuclear nickel(II) precursor motifs.

FT-IR Spectra. The presence of nickel-bound terminal alcohol and bridging HO^- groups and lattice water molecules in $\mathbf{1}{\cdot}H_2O{\cdot}2DMF$, $\mathbf{2}{\cdot}4H_2O$, and $\mathbf{3}{\cdot}9H_2O$ is manifested by one broad band of medium intensity at 3485, 3464, and 3429 cm^{-1}, respectively, for the three complexes and assigned to $\bar{\nu}_{OH}$ stretching frequencies (Figure S1 in the SI). The $\bar{\nu}_{C=N}$ and $\bar{\nu}_{C=O}$ stretching frequencies from the phenol-deprotonated bis-Schiff base H_2L^-, hydrolyzed and phenol-deprotonated mono-Schiff base $^{hy}HL^-$, and fully deprotonated L^{3-} are observed within 1639−1652 cm^{-1} for the three complexes. For **1**, asymmetric ($\bar{\nu}_{as(COO)}$) and symmetric ($\bar{\nu}_{s(COO)}$) stretching vibrations of the two pivalate groups are detected at 1567

DOI: 10.1021/acs.inorgchem.5b00039
Inorg. Chem. 2015, 54, 4709−4723

and 1388 cm^{-1}, respectively, with a difference ($\Delta\bar{\nu} = \bar{\nu}_{as(COO)} - \bar{\nu}_{s(COO)}$) of 179 cm^{-1}. This difference is in agreement with the presence of $\mu_{1,3}$-carboxylato bridges between the Ni^{II} sites in **1** to sustain the clusterlike assembly of metal ions and ligands. At this point, it is worth noting that nonbridging monodentate carboxylate coordination would lead to a greater separation of ca. 350 cm^{-1}.[46] The very strong band at 1384 cm^{-1} for **1** is attributed to the $\nu_3(E')$ mode of the NO_3^- group, indicating the presence of two ionic nitrates required for fulfilling the dicationic charge of the complex.[47] For **2**, the corresponding positions in the FT-IR spectrum are at 1559 ($\bar{\nu}_{as(COO)}$) and 1406 cm^{-1} ($\bar{\nu}_{s(COO)}$) for bound propanoate groups in $\mu_{1,3}$ mode with a $\Delta\bar{\nu}$ value of 153 cm^{-1}.[29,30] In addition, complex **2** shows a strong band at 2066 cm^{-1}, which is assigned to the asymmetric stretching vibration, ν_{as}(NNN), of the end-on azide group needed for the sustainability of the dicubane structure.[48] The FT-IR spectrum of **3** exhibits a strong band at 1058 cm^{-1} and a medium band at 622 cm^{-1}, due to the $\nu_3(F_2)$ (ν_{ClO}) and $\nu_4(F_2)$ (δ_{dOClO}) modes, respectively, of the uncoordinated tetrahedral ClO_4^- ions.[47] The IR stretching bands characteristic of a coordinated carbonate ion are observed at 1449 and 836 cm^{-1}, which are typical for ligand binding metal ions in the μ_6 form.[49] The identical composition in the solid state of the powder and single-crystalline products of the three compounds has been well monitored and compared for their characteristic band positions using FT-IR spectroscopy and powder X-ray diffraction (PXRD). The PXRD data have been taken to identify and characterize the individual phases of solid crystalline **1**·H_2O·2DMF, **2**·$4H_2O$, and **3**·$9H_2O$. The PXRD patterns of the three compounds are shown in Figures S2−S4 in the SI. These patterns are well consistent with those of the simulated ones obtained from the single-crystal X-ray diffraction data. Both the 2θ values corresponding to lattice spacing and the relative intensity of the diffraction lines are indicative of the particular phase of the compounds.

Electronic Spectra. All of the compounds are moderately soluble in MeOH, and the solutions suitable for recording the electronic absorption bands in the UV−vis region allowed us to record from 200 to 800 nm. Broad absorption bands (λ), with maxima at 663 nm (ε = 120 L mol^{-1} cm^{-1}), 674 nm (ε = 400 L mol^{-1} cm^{-1}), and 673 nm (ε = 415 L mol^{-1} cm^{-1}) for **1**·H_2O·2DMF, **2**·$4H_2O$, and **3**·$9H_2O$, respectively, can be assigned to the spin-allowed $^3A_{2g}(F) \rightarrow {}^3T_{1g}(F)$ transition consistent with their slightly distorted octahedral configurations. The $^3A_{2g}(F) \rightarrow {}^3T_{2g}(F)$ transition that usually appears above 700 nm is systematically missing for all three complexes.[50] The absorptions at 372 nm (ε = 8184 L mol^{-1} cm^{-1}), 405 nm (ε = 9743 L mol^{-1} cm^{-1}), and 400 nm (ε = 2389 L mol^{-1} cm^{-1}) correspond to the $^3A_{2g}(F) \rightarrow {}^3T_{1g}(P)$ transitions for the three complexes, respectively.[51] The intense absorptions below 300 nm at 254 nm (ε = 39273 L mol^{-1} cm^{-1}), 246 nm (ε = 27613 L mol^{-1} cm^{-1}), and 258 nm (ε = 61561 L mol^{-1} cm^{-1}) are the result of Ni^{II}-bound ligand-based absorptions.

Description of the Crystal Structures. Single crystals of **1**·H_2O·2DMF were obtained after 1 month from a saturated DMF solution. For **2**·$4H_2O$ and **3**·$9H_2O$, suitable single crystals for X-ray structure determination were obtained by the slow evaporation of saturated MeOH solutions of these two compounds after 1 week.

***1**·H_2O·2DMF.* The crystal structure of compound **1** is shown in Figure 1, and important bond lengths and angles are provided in Table S1 in the SI. Compound **1**·H_2O·2DMF crystallizes in the triclinic $P\bar{1}$ space group with two molecules in the unit cell. The structure consists of a tetrametallic dicationic part, $[Ni_4(\mu_3\text{-}OH)_2(H_2L)_2(\mu_{1,3}\text{-}{}^tBuCO_2)_2]^{2+}$, and the corresponding nitrate counteranions. The tetranuclear complex consists of two deprotonated H_2L^- ligands, each of them delivering a set of N_2O_3 donor atoms to the $[Ni_4]$ complex that assembles around two μ_3-OH groups at two vertices of the cube. Two pivalate groups complete the coordination environments around each Ni^{II} site (Figure 1). Two HO^- anions, O8 and O9, at the corner of the cube help to organize the four Ni^{II} ions in a distorted tetrahedral geometry, with the Ni···Ni distances varying from 2.895 to 3.297 Å (Figures S6 and S7 in the SI; these distances are longer than the known double phenoxido- and phenoxido−hydroxido-bridged nickel dimers[52]). The Ni−O distances vary within the 1.992−2.253 Å range versus the Ni−N distances at 2.001−2.011 Å. The identification of two short (2.040 and 2.092 Å) Ni−O_{ph} bonds and one long (2.222 Å) bond, forming a *dimer-of-dimer* aggregation, in the structure clearly indicates the formation of complex **1** through the aggregation of two dinuclear fragments (Figure S5 in the SI).

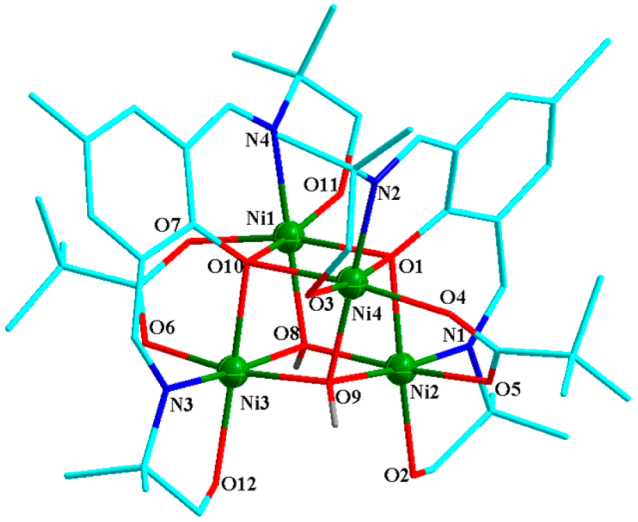

Figure 1. View of the tetranickel cubane unit $[Ni_4(\mu_3\text{-}OH)_2(H_2L)_2(\mu_{1,3}\text{-}O_2CBu^t)_2]^{2+}$ in **1** with a partial atom-numbering scheme. H atoms (except two bridging hydroxido groups), noncoordinated nitrate ions, and solvent molecules are omitted for clarity. Color code: Ni, green; N, blue; O, red; C, cyan; H, gray.

While the HO^- bridging modes present in this complex are quite common, the μ_3-phenoxido feature observed in **1** for growth of the cubane complex is rather exceptional. Two types of μ_3-bridges by phenoxido and hydroxido groups show different magnitudes of Ni−O−Ni angles in the 88.93−106.31° range. Two of the six faces of the $[Ni_4O_4]$ cube are distinctly different, being spanned by capping pivalates. The Ni···Ni distances on the pivalate bridging faces are 2.895 and 2.922 Å. The double phenoxido-bridged face registers a Ni···Ni separation of 3.297 Å, which is different from the double hydoxido-bridged face at 3.122 Å. In the remaining two faces, the Ni···Ni nonbonding distances are 2.895 and 3.233 Å (Figure S7 in the SI). In the case of μ_3-phenoxido bridging, one Ni−O−Ni angle is close to 90° (Ni1−O1−Ni4, 88.93°; Ni1−O10−Ni4, 89.30°), whereas the other two are well above the same (95.50−101.25°). The same is true for the μ_3-hydroxido template holding the cubane structure (Ni−O_{hy}−Ni angles vary between 92.11 and 106.31°). The side-by-side presence of

DOI: 10.1021/acs.inorgchem.5b00039
Inorg. Chem. 2015, 54, 4709−4723

octahedral Ni and tetrahedral O atoms is mainly responsible for the cubane distortion.

The cationic complex crystallizes with two nitrate anions, one water, and two DMF molecules, which are hydrogen-bonded to ligand alcohol arms. These hydrogen-bonding interactions provide an aesthetically pleasing crystal packing (Figure S8 in the SI).

***2**·4H$_2$O.* The molecular structure of **2**·4H$_2$O is shown in Figure 2, and selected bond lengths and angles are listed in

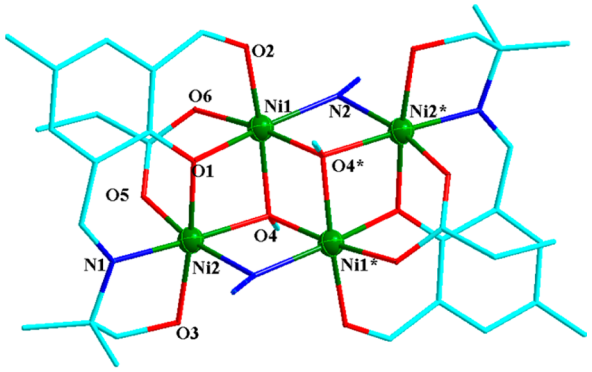

Figure 2. View of [Ni$_4$(μ-^{hy}HL)$_2$(μ_3-OMe)$_2$($\mu_{1,1}$-N$_3$)$_2$($\mu_{1,3}$-CO$_2$Et)$_2$] in **2** with a partial atom-numbering scheme. Water molecules and H atoms are omitted for clarity. Symmetry operation: *, 1 − *x*, −*y*, 1 − *z*. Color code: same as that in Figure 1

Table S2 in the SI. Complex **2** crystallizes in the triclinic $P\bar{1}$ space group, and the asymmetric unit contains only half of the tetranuclear complex, with the second half being generated by the (1 − *x*, −*y*, 1 − *z*) symmetry transformation. The formula of **2**·4H$_2$O contains two ^{hy}HL$^-$ ligands (Scheme 2), which originate from the hydrolysis of one of the arms of H$_2$L$^-$, as assisted presumably by the coordination of Ni^{II} ions followed by the aggregation of two such fragments. There are two crystallographically inequivalent, but nearly identical, tetranuclear complexes per unit cell. The three-dimensional arrangement of the [Ni$_4$N$_2$O$_4$] core has the shape of a defective face-shared dicubane where one vertex is missing from each cube. A similar [Ni$_4$] unit having dicubane topology was found in other nickel complexes with phenol-based ligands.[53] The tetranuclear dicubane complex consists of two hydrolyzed and singly deprotonated ^{hy}HL$^-$ ligands, each of them delivering a set of NO$_3$ donor atoms to the [Ni$_4$] complex that assembles on two μ_3-MeO$^-$ centers with peripheral supports from two μ-N$_3^-$ and two μ-EtCO$_2^-$ in a centrosymmetric arrangement (Figure S10 in the SI). Two types of octahedral NO$_5$ and N$_2$O$_4$ coordination spheres are found around Ni1, Ni1* and Ni2, Ni2*, respectively. In the case of the first type, Ni1 and Ni1* form a Ni$_2$O$_2$ diamond unit with bridging methoxido O atoms (O4 and O4*), together with coordination from phenoxido (O1), carboxylato (O6), and aldehydo (O2) O and azido (N2) N atoms. The latter environment is completed by methoxido (O4), phenoxido (O1), carboxylato (O5), and alcohol (O3) O atoms and azido (N2) and imine (N1) N atoms. The Ni···Ni distances in five faces of the dicubane are different. Two of the five faces of the partial dicubane are triply bridged and spanned by the capping of propanoates, which result in somewhat different bond lengths and angles for the involved atoms compared to those at the three remaining faces (Figures S9 and S10 in the SI). Within these faces as well as for the terminal ligations, the Ni−O distances in the 2.004−2.060 Å range are close to the Ni−N separations at 2.011−2.149 Å.

For unsymmetrical azide coordination, the identification of one short (2.096 Å) and one long (2.149 Å) Ni−N$_{az}$ bond in the structure clearly indicates the formation of the tetranuclear complex through the aggregation of two [Ni$_2$] fragments supported by the μ_3-bridge extension of two methoxido groups (Scheme S5 in the SI). The distorted octahedral environments around each Ni^{II} ion are reflected from variation of the cis and trans angles in the 79.3−102.7 and 169.4−177.9° range, respectively (Table S2 in the SI). The adjacent Ni−O−Ni angles around μ_3-methoxido bridges show considerable variation within the 92.3−102.9° range. Both metal-bound aldehyde and alcohol functions of the ligand are engaged in hydrogen-bonding interactions with the lattice water molecule per formula unit of the complex (Figure S11 in the SI).

***3**·9H$_2$O.* The block-shaped crystal used in molecular structure determination crystallizes in the monoclinic $P2_1/c$ space group with four molecules in the unit cell. The asymmetric unit contains the entire cluster as well as one perchlorate anion and eight lattice water molecules. The molecular structure of **3** is shown in Figure 3, and selected

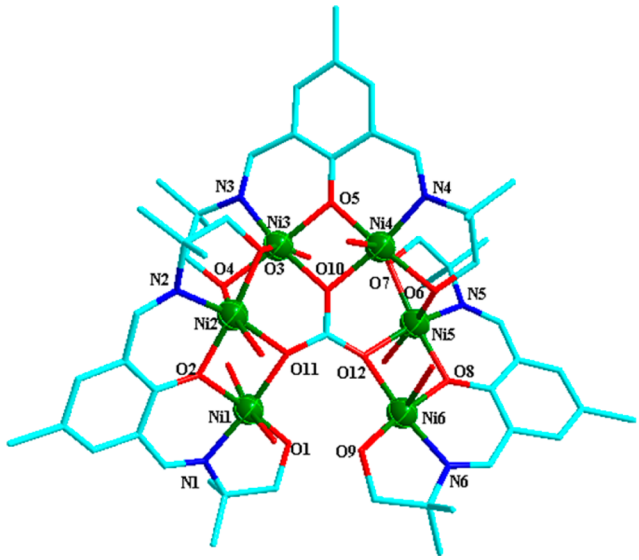

Figure 3. View of the [Ni$_6$(μ_4-L)(μ_3-L)$_2$(μ_6-CO$_3$)(H$_2$O)$_8$]$^+$ unit in **3** with a partial atom-numbering scheme. H atoms, perchlorate ion, and water molecules are omitted for clarity. Color code: same as that in Figure 1

bond lengths and angles are listed in Table S3 in the SI. The cationic complex features six Ni^{II} ions disposed in a planar quasi-ideal hexagonal arrangement around a central carbonato anion. The [Ni$_6$] complex results from the assembly of three [Ni$_2$(μ-L)]$^+$ fragments around the central CO$_3^{2-}$ group with support from terminal alkoxido O atoms (Figure S12 in the SI). Each L^{3-} unit binds two metal ions, and three such [Ni$_2$L]$^+$ units assemble around the CO$_3^{2-}$ group, which adopts a rare μ_6:η_2:η_2:η_2 bridging mode. It may best be described as an octahedron with four nearly coplanar Ni^{II} ions (Ni1, Ni3, Ni4, and Ni6), with the remaining two ions (Ni2 and Ni5) lying above and below the Ni$_4$ plane (Figure 4).

The most important feature of the structure is the μ_6-carbonato bridge situated near the center of the [Ni$_6$] core, which helps to assemble and aggregate three binuclear

DOI: 10.1021/acs.inorgchem.5b00039
Inorg. Chem. 2015, 54, 4709−4723

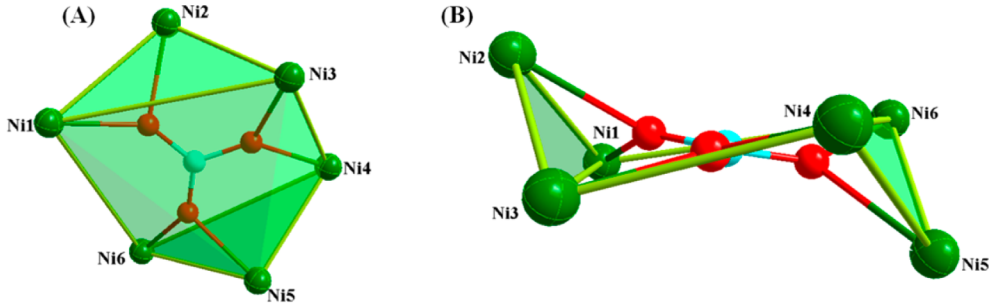

Figure 4. (A) Central carbonato support for the hexanuclear arrangement and (B) side chair view of the same.

fragments with an overall cationic charge to the complex. All six Ni^{II} ions within the $[Ni_6O_{10}]$ core are in a distorted octahedral NO_5 coordination environment. In the case of Ni2, Ni3, Ni4, and Ni5, the octahedral coordination sphere is assembled from carbonato, phenoxido, alkoxido, and water O and imine N atoms. The Ni^{II} atoms at the open edge of the pentagon (Ni1 and Ni6) have different types of O atom environments compared to the other four atoms. Within these environments, the Ni−O distances in the 1.999−2.269 Å range are close to the Ni−N separations at 1.962−1.993 Å. The distorted NO_5 octahedral environment around each Ni^{II} ion is reflected from variation in the cis and trans angles from 78.9 to 105.3° and from 162.8 to 175.3°, respectively (Table S3 in the SI). The hexanuclear complex consists of three completely deprotonated L^{3-} ligands, each of them delivering a set of N_2O_3 donor atoms to the $[Ni_6]$ complex that assembles on and around the central μ_6-CO_3^{2-} ion (Figure S12 in the SI). The Ni···Ni distances within the $[Ni_2(\mu\text{-L})]^+$ fragments fall in the 3.080−3.142 Å range, which are longer than the double alkoxido-bridged interdimeric Ni···Ni separations within 2.909−2.925 Å. Interestingly, the former units are doubly bridged in a phenoxido support, whereas the latter show triple bridge support from two alkoxido groups and one carbonato unit. The open edge of the nonplanar hexagon records the longest Ni···Ni distance of 4.535 Å (Figure S13 in the SI). The six Ni−O bonds from the encapsulated carbonato group are within the 1.999−2.133 Å range, while the C−O bond lengths of the group remain within 1.270−1.297 Å. The different coordination environments lead to subtle differences in the Ni−O bonding distances, leading to elongation of the O−Ni−O axes made from aqua and alkoxide coordination perpendicular to the Ni_2O_2 diamond cores formed from phenoxido and carbonato bridging. Interestingly, intermolecular hydrogen-bonding interactions are found between the crystallizing water molecules and the counterion (Figure S14 in the SI).

Magnetic Properties. The temperature dependence of the magnetic properties of powdered polycrystalline samples of **1**−**3** under a constant magnetic field of 0.1 T in the 2−300 K range is represented in the form of $\chi_M T$ versus T plots (χ_M being the molar paramagnetic susceptibility of the compound) in Figures 5−7, respectively. At room temperature, the $\chi_M T$ values for complexes **1**−**3** (5.40, 5.48, and 7.44 $cm^3\ mol^{-1}\ K$, respectively) are significantly higher than that expected for uncoupled Ni^{II} ions (S = 1) with g = 2.0 (4.0 $cm^3\ mol^{-1}\ K$), which is mainly because of the orbital contribution of the Ni^{II} ions.

As can be observed in Figure 5, the $\chi_M T$ product of **1** slightly increases with decreasing temperature to reach a rounded maximum at 50 K (5.62 $cm^3\ mol^{-1}\ K$) and then decreases to

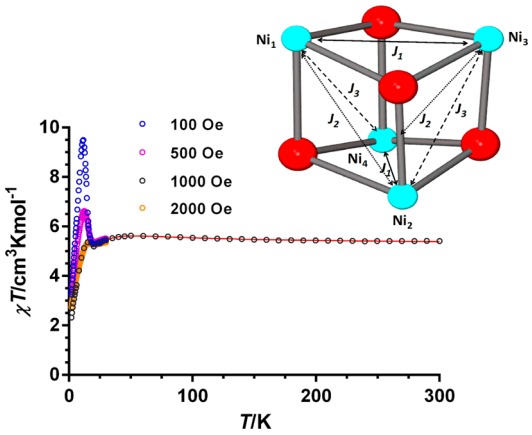

Figure 5. Temperature dependence of $\chi_M T$ for **1** at different magnetic fields. The red solid line is generated from the best fit magnetic parameters. Inset: coupling scheme for **1**. Temperature dependence of the molar out-of-phase ac susceptibility (χ_M'') for **1** under zero dc applied field at different frequencies.

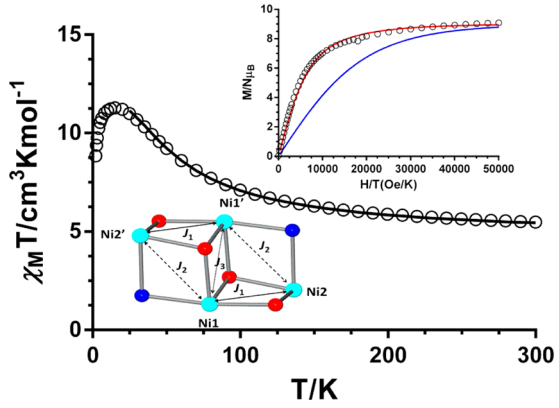

Figure 6. Temperature dependence of $\chi_M T$ for **2**. The solid line is generated from the best fit magnetic parameters. Inset top: Field dependence of the magnetization for **2**. The red and blue solid lines represent Brillouin functions for an S = 4 ground state and for the sum of four Ni^{II} ions with S = 1, respectively. Inset bottom: Coupling scheme for **2**.

attain a minimum at 20 K with a value of 5.20 $cm^3\ mol^{-1}\ K$. This behavior clearly indicates the existence of both ferromagnetic and antiferromagnetic interactions in this compound. Below 20 K, the $\chi_M T$ product undergoes an abrupt increase to reach a maximum at 15 K (5.36 $cm^3\ mol^{-1}\ K$) and then sharply decreases to a value of 2.32 $cm^3\ mol^{-1}\ K$ at 2 K. It should be noted that the intensity of the maximum increases when the applied magnetic field decreases, which could be due

DOI: 10.1021/acs.inorgchem.5b00039
Inorg. Chem. 2015, 54, 4709−4723

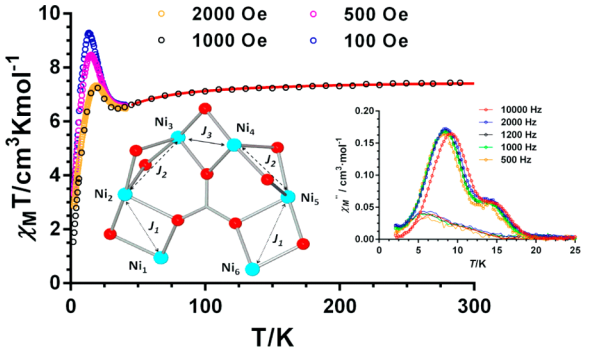

Figure 7. Temperature dependence of $\chi_M T$ for **3** at different fields. The solid red line is generated from the best fit magnetic parameters above 45 K. Inset left: Coupling scheme for **3**. Inset right: Temperature dependence of the molar out-of-phase ac susceptibility (χ_M'') for **3** under zero dc applied field (circles) and 1000 Oe (solid lines) at different frequencies.

to either spin-canting antiferromagnetism or spin-glass behavior. It should be highlighted at this point that we have carried out several preparations of **1** and all of the crystalline samples exhibited the same behavior. Dynamic ac measurements under zero applied magnetic field reveal the presence of a slightly frequency-dependent out-of-phase signal (χ_M'') with maxima in the temperature range of 10.9−11.5 K. We have analyzed the frequency-dependent shift of the maxima using the Mydosh empirical parameter $\gamma = (\Delta T_f/T_f)/\Delta(\log f)$, where T_f is the temperature corresponding to the maximum in the χ_M'' versus T curve for each frequency (f) and ΔT_f is the difference between the highest and lowest temperatures corresponding to the extremes of the frequency range under exploration.[54] The calculated shift parameter $\gamma = 0.042$ falls in the range expected for spin glasses and rules out the SMM behavior for **1**. In fact, in all of the Ni_4O_4 cubane complexes that show relaxation of the magnetization and SMM behavior, the out-of-phase signal presents maxima that appear at much lower temperatures than those in **1**.[55] It should be noted that the out-of-phase signal vanishes when a magnetic field of 1000 Oe is applied. This behavior is compatible with spin-canted systems as well as with spin glasses. Nevertheless, the presence of an inversion center and the parallel alignment of the pseudo-2-fold axis of the cubane molecules in the structure of **1**, as well as the frequency dependence of the out-of-phase signal, seem to discard the spin-canting mechanism. It is worth mentioning that, to observe the spin-glass collective behavior, considerable intercluster interactions are mandatory. However, the Ni_4O_4 clusters in **1** are rather well separated (the smaller Ni···Ni distance is 9.575 Å), and no exchange pathways are apparent from the crystal structure, so that only weak dipole−dipole interactions are possible. Nevertheless, these weak interactions are hardly expected to be responsible for the spin-glass behavior. An alternative explanation to the origin of the surprising low-temperature magnetic behavior of **1** could be found in the existence of a trace amount of either an extended metal complex or a disordered structure with nonnegligible intercluster interactions obtained by the loss of crystallization solvent molecules in the structure of **1**. Interestingly, the presence of possible impurifying metal complexes was not detected from PXRD (see Figure S2 in the SI). It should be noted that a similar magnetic behavior was also observed for other discrete nickel(II) complexes.[11,56] In some cases, it was ascribed to spin-glass behavior[56a,b] and in other cases to the additional presence of trace amounts of either desolvated compounds with disordered structures[11] or NiO nanoparticles.[56c]

In keeping with the cubane structure of **1**, the experimental susceptibility data were analyzed by using the following isotropic spin-Heisenberg Hamiltonian:

$$H = -J_1(S_{Ni1}S_{Ni3} + S_{Ni2}S_{Ni4}) - J_2(S_{Ni1}S_{Ni2} + S_{Ni3}S_{Ni4}) - J_3(S_{Ni1}S_{Ni4} + S_{Ni2}S_{Ni3})$$

where J_1, J_2, and J_3 describe the exchange pathways through the μ_3-phenoxido/μ_3-hydroxido/*syn*−*syn*-^{t}BuCO$_2^-$, μ_3-phenoxido/μ_3-hydroxido, and double-μ_3-phenoxido/double-μ_3-hydroxido bridging pathways, respectively. Only data above the minimum, in the temperature range 25−300 K, were fitted with the above Hamiltonian. The best fit led to the following set of parameters: $J_1 = +11.4$ cm^{-1}, $J_2 = -2.1$ cm^{-1}, $J_3 = -2.8$ cm^{-1}, and $g = 2.30$ with $R = 1.3 \times 10^{-7}$ ($R = \sum[(\chi_M T)_{exp} - (\chi_M T)_{calcd}]^2/\sum(\chi_M T)_{exp}^2$).

As expected for the antiferromagnetic interaction operating at low temperature, the field dependence of the molar magnetization at 2 K for compound **1** (Figure S15 in the SI) is well below the Brillouin function for the sum of the contribution of four isolated Ni^{II} ions and does not achieve saturation even at the highest applied field of 5 T.

The $\chi_M T$ product of **2** steadily increases when the temperature is decreased, reaching a maximum at 15 K (11.28 cm^3 mol^{-1} K). Below the temperature of the maximum, $\chi_M T$ decreases to reach a value of 8.84 cm^3 mol^{-1} K at 2 K. This behavior points out the existence of significant intramolecular ferromagnetic couplings between the Ni^{II} ions, leading to a $S = 4$ ground state. The decrease in $\chi_M T$ at low temperatures is more likely due to the ZFS effects of the ground state and/or intermolecular antiferromagnetic interactions. The experimental susceptibility data for **2**, with a centrosymmetric face-sharing defective dicubane-like structure, were modeled with the following three-J Hamiltonian (see the inset in Figure 6):

$$H = -J_1(S_{Ni1}S_{Ni2} + S_{Ni1}S_{Ni2'}) - J_2(S_{Ni1}S_{Ni2} + S_{Ni1}S_{Ni2'}) - J_3(S_{Ni1}S_{Ni1'})$$

where J_1, J_2, and J_3 describe the exchange pathways through μ-phenoxo/μ_3-methoxide, μ-azide/μ_3-methoxide, and μ_3-methoxide/μ_3-methoxide, respectively. The D and zJ' parameters accounting for the local anisotropy of the Ni^{II} ions and the intermolecular interactions, respectively, were not included in the Hamiltonian to avoid overparametrization. As a consequence, only data above 25 K that are not affected by the effects of D and zJ' were fitted with the above Hamiltonian. The best fit led to the following set of parameters: $J_1 = +27.5$ cm^{-1}, $J_2 = +20.62$ cm^{-1}, $J_3 = +1.52$ cm^{-1}, and $g = 2.17$ with $R = 1.7 \times 10^{-6}$.

The field dependence of the molar magnetization at 2 K for compound **2** (inset in Figure 6) is above the Brillouin function for the sum of the contribution of four isolated Ni^{II} ions (blue line) and is almost coincident with the Brillouin function for a $S = 4$ ground state (red line), which corroborates the existence of ferromagnetic interaction between the Ni^{II} ions.

$$M = NgBs(y); \quad y = g\beta SH/kT$$

$$Bs(y) = \frac{2S+1}{2S}\coth\left(\frac{2S+1}{2S}y\right) - \frac{1}{2S}\coth\left(\frac{1}{2S}y\right)$$

DOI: 10.1021/acs.inorgchem.5b00039
Inorg. Chem. 2015, 54, 4709−4723

Table 2. Magnetic Exchange Constant Values, J (cm^{-1}), for Cubane-like Tetramers

compound	Ni−O−Ni angle (deg)	exchange pathway	J	g	ref
$[Ni_4(\mu_3\text{-}OH)_2(\mu_3\text{-}H_2bpmp)_2(\mu_{1,3}\text{-}O_2CCF_3)_2]^{2+}$		hydroxido	9.3	2.27	11
		alkoxido	1.1		
$[Ni_4(\mu_3\text{-}OMe)_4(Q)_4(MeOH)_4]$	95.9	methoxido	3.4	2.24	12b
	100.0	alkoxido	−1.8		
$[Ni_4(MeOH)_4L_4]$	93.1−97.4	alkoxido	8.0	2.22	compound **1** in12c
	100.1−101.2		−3.0		
$[Ni_4(\mu_3\text{-}OMe)_4(L_2)_4(MeOH)_4]$	96.5−98.3	methoxido and alkoxido	5.6	2.2	compound **6** in12d
$[Ni_4(HL^1)_3(HL^2)(H_2O)(CH_3OH)]$ $[AcO]\cdot 2CH_3OH\cdot CH_3CN$	99	alkoxido	15.96	2.43	12e
		phenoxido	4.11		
$[Ni_4(cit)_4]$ $[C(NH_2)_3]_8\cdot 8H_2O$	96.9	alkoxido	2.97	2.30	12f
	99.7		−0.3		
$[Ni_4(H_4L)(H_3L)(acac)_2][OAc]$	96.3	alkoxido	10.2	2.10	compound **1** in12g
	98.1	phenoxido	2.4		
$[Ni_4(L_2)_4(H_2O)(MeOH)_3]$	96.7	alkoxido	7.35	2.06	12h
	99.9	phenoxido	−2.55		
$[Ni_4(hfac)_4(OMe)_4(MeOH)_4]$	96.2	alkoxido	9.2	2.32	19b
	98.2	phenoxido	4.4		
$[Ni_4(L)_2(HL)_2(SeCN)_2(H_2O)_2]\cdot C_3H_7NO\cdot 4H_2O$	96.8	alkoxido	6.87	2.15	compound **2** in15b
	98.0	alkoxido/phenoxido	4.62		
	103.4	phenoxido	−5.14		
$[Ni_4L_4(MeOH)_4]\cdot H_2O$	96.5	alkoxido	8.90	2.22	12i
	100.2	phenoxido	−5.63		
$[Ni_4(\mu\text{-}OMe)_4(O_2CArTol)_4(MeOH)_6]_{1.5}(MeOH)_3$	95.0−96.4	methoxido	17.4	2.22	12j
	97.8−98.6		13.6		
$[Ni_4(EtOH)_3L_4]$	96.1	alkoxido	7.15	2.14	12k
	98.5	phenoxido	−0.34		
$[Ni_4(\mu_3\text{-}OH)_2(H_2L)_2(\mu_{1,3}\text{-}O_2CBu^t)_2]\cdot(NO_3)_2\cdot H_2O\cdot 2DMF$	90.7	alkoxido	11.4	2.30	compound **1** in this work
	101.0	hydroxido	−2.1		
	100.1	phenoxido	−2.8		

The M versus H plot can be well reproduced with the parameters extracted from the fit of the susceptibility data with $g = 2.23$.

In order to know whether **2** exhibits slow relaxation of the magnetization and SMM behavior, ac magnetic susceptibility measurements as a function of the temperature and frequency (between 10 and 1000 Hz) were performed under 0 and 1000 Oe direct-current (dc) fields. The results of these measurements demonstrate that this compound does not exhibit a frequency dependence of the out-of-phase (χ''_M) signals above 2 K, and therefore it does not behave as a SMM magnet. This could be due to either an almost negligible axial anisotropy (D) of the ground state (in fact, the M vs H plot is almost coincident with the Brillouin function for an isotropic $S = 4$ state) or a $D > 0$ value.

As can be seen in Figure 7, $\chi_M T$ for **3** steadily decreases with decreasing temperature until a minimum at 35 K (6.5 cm^3 mol^{-1} K) is reached, thus suggesting the existence of a predominant antiferromagnetic interaction. Below this temperature, $\chi_M T$ sharply rises to attain a maximum at 20 K (7.5 cm^3 mol^{-1} K) and then brusquely decreases to a value of 1.54 cm^3 mol^{-1} K at 2 K. The magnetic behavior below 35 K for **3** is similar to that observed for **1**, but the field-dependent maximum (see Figure 7) appears at a higher temperature. ac measurements under zero applied magnetic field point out that the out-of-phase signal (χ_M'') exhibits a small frequency dependence with maxima in the temperature range of 8.5−9.25 K and shoulders at about 14.25 K. The Mydosh parameter for the former is $\gamma = 0.06$. When a static magnetic field of 1000 Oe is applied, the out-of-phase signals (χ_M'') dramatically decrease but do not fully vanish. Because the compound exhibits a center of symmetry, this behavior would be, in principle, only compatible with spin-glass behavior. In the case of **3**, there exists an extensive hydrogen-bonding network involving the hexanuclear Ni6 molecules, crystallization water molecules, and MeOH molecules, and the shortest Ni···Ni intercluster distance (8.611 Å) is smaller than that found in **1**. Therefore, significant intercluster magnetic interactions are expected in **3**, which could be responsible for the observed spin-glass behavior occurring at higher temperature than in **1**. Nevertheless, we consider as the most probable scenario the existence, like in the case of **1**, of a trace amount of either an extended metal complex or a disordered structure with nonnegligible intercluster interactions, obtained by the loss of crystallization solvent molecules in the structure of **3**, which would be responsible for the observed magnetic behavior at low temperature.

Evaluation of the coupling constant in **3** is a very complex task because there are many exchange coupling pathways including not only mixed ligand/carbonate bridges but also those involving only the carbonato bridging ligand (Ni6/Ni3, Ni1/Ni4, Ni2/Ni6, Ni1/Ni5/Ni2/Ni4, Ni3/Ni5, and Ni1/Ni6). Among them, those connecting nonneighboring Ni^{II} atoms usually transmit weak magnetic interactions.[57] Moreover, the fact that the above-indicated exchange pathways connect Ni^{II} atoms that are not in the plane of the carbonato-bridging ligand reduces the extent of the overlap between the magnetic orbitals of the Ni^{II} atoms, thus leading to very weak

DOI: 10.1021/acs.inorgchem.5b00039
Inorg. Chem. 2015, 54, 4709−4723

Table 3. Magnetic Exchange Constant Values, J (cm^{-1}), for Dicubane-like Tetramers

compound	exchange pathway	J_1	J_2	J_3	g	ref
$[Ni_4(\mu_2\text{-}N_3)_4(\mu_3N_3)_2(N_3)_2(enbzpy)_2]\cdot 2H_2O$	azido	15.8	15.8	14.6	2.15	17b
$[Ni_4(dpk\cdot OH)_3(dpk\cdot CH_3O)_2(NCO)](BF_4)_2\cdot 3H_2O$	hydroxido and methoxido	6.9	7.0	15.2	2.06	13b
$[Ni_4L_2(\mu_3\text{-}OMe)_2(H_2O)_2]\cdot 2H_2O$	phenoxido, methoxido, and alkoxido	13.4	9.8		2.14	13c
$[Ni_4(H_2O)_2(PW_9O_{34})_2]^{10-}$	alkoxido	6.5	6.5	2.5	2.12	13d.
$[Ni_4(dpk\cdot OH)_4(N_3)_4]$	azido and alkoxido	18.8	6.9	1.8	2.13	13e
$[Ni_2(dpk\cdot(O)(OH)(dpk\cdot(O)(OCH_3)(N_3)_2]_2$	alkoxido, azido, and hydroxido	7.07	7.08	11.4	2.1	13f
$[Ni_4(H_2L)_2(OCH_3)_2(CH_3CO_2)_2(N_3)_2]$	phenoxido, methoxido, and azido	29.5	11.6	11.6	2.11	53a
$[Ni_4(\mu\text{-}^{hy}HL)_2(\mu_3\text{-}OMe)_2(\mu_{1,1}\text{-}N_3)_2(\mu_{1,3}\text{-}O_2CEt)_2]\cdot H_2O$	phenoxido, methoxido, and azido	27.5	20.6	1.52	2.17	compound **2** in this work

Table 4. Magnetic Exchange Constant Values, J (cm^{-1}), for Carbonate-Bridged Nickel(II) Complexes

compound	exchange pathway	J_1	J_2	J_3	J_4	g	ref
$[Ni_8(\mu\text{-}H_2bpmp)_4(\mu_4\text{-}CO_3)_4(ImH)_8](NO_3)_4\cdot 2H_2O$	phenoxido and carbonato	3.0	0.4	−7.5	2.24		4c
$[Ni_6(CO_3)(N_3)_6\{pyCOpyC(O)(OMe)py\}_3(MeOH)_2(H_2O)]$ $[Ni_6(CO_3)(N_3)_6\{pyCOpyC(O)(OMe)py\}_3(MeOH)_3](ClO_4)_2$	alkoxido and carbonato	6.1	27.0			2.18	30
$\{K[Ni_6(\mu_6\text{-}CO_3)(\mu_{1,1}\text{-}N_3)_6(\mu\text{-}OAc)_3(dpkMeCN{-}H)_3]\}_2[K_2(H_2O)_2]\cdot$ $3MeCN\cdot 7H_2O$	carbonato, azido, and acetato	2.88	25.4	0	0	2.28	31
$[Ni^{II}_{12}(trans\text{-}tachH)_6(OMe)_{12}(OAc)_9(CO_3)](OAc)_7\cdot 10MeOH\cdot 6H_2O$	carbonato, acetato, carbonato, oxo, and methoxido	−17.5	9.5	1.9	22.0	2.21	compound **2** in 32
$[Ni_6(\mu_4\text{-}L)(\mu_3\text{-}L)_2(\mu_6\text{-}CO_3)(H_2O)_8](ClO_4)\cdot 8H_2O$	phenoxido and carbonato	−3.3	1.7	−12.8		2.24	compound **3** in this work

magnetic exchange interactions, even in the case of the Ni1/N6 pathway. In view of this, we decided to analyze the susceptibility data above 45 K for **3** with the following crude three-J isotropic Hamiltonian (see the inset in Figure 7):

$$H = -J_1(S_{Ni1}S_{Ni2} + S_{Ni5}S_{Ni6}) - J_2(S_{Ni2}S_{Ni3} + S_{Ni4}S_{Ni5}) - J_3(S_{Ni3}S_{Ni4})$$

where J_1, J_2, and J_3 describe the magnetic exchange pathways through the double bridges μ-phenoxido/μ-carbonate, the triple bridges μ-alkoxido/μ-alkooxido/μ-*syn*−*syn* carbonate, and the double bridges μ-phenoxido/μ-carbonato, respectively. In order to avoid overparametrization, the very weak interactions between Ni^{II} ions belonging to different arms of the ligand through the carbonato bridging group were not considered. The best fit of the experimental susceptibility data to the above Hamiltonian afforded the following parameters: $J_1 = -3.30$ cm^{-1}, $J_2 = +1.7$ cm^{-1}, $J_3 = -12.8$ cm^{-1}, and $g = 2.24$ with $R = 3.4 \times 10^{-7}$.

As for **1**, the field dependence of the molar magnetization at 2 K for compound **3** (Figure S16 in the SI) is well below the Brillouin function for the sum of the contribution of six isolated Ni^{II} ions and is far from being saturaed at the highest applied magnetic field of 5 T.

Magnetostructural Correlations. The key factor controlling the sign and magnitude of the magnetic exchange coupling in planar $Ni(O)_2Ni$ dinuclear complexes (O belonging to hydroxido, alkoxido, and phenoxido bridging groups) is the Ni−O−Ni bridging angle (θ).[58] Thus, a ferromagnetic coupling is expected for θ values close to 90°. As the θ angle increases from this value, the ferromagnetic coupling decreases and turns into antiferromagnetic at values of ∼96−98°. Moreover, the antiferromagnetic interaction increases when the τ (the out-of-plane displacement of the phenyl C atom from the Ni_2O_2 plane in alkoxido- and phenoxido-bridged complexes)[26] and β (hinge angle between the O−Ni−O planes in the bridging region) angles decrease. The relationship between the Ni−O−Ni angle and exchange constant for similar Ni_4 cubane-like complexes is summarized in Table 2. Moreover, it has been recently shown that the *syn*−*anti*-carboxylate bridge promotes in diphenoxide-bridged nickel(II) complexes enhanced ferromagnetic interactions by a countercomplementarity effect.[59] In view of these magnetostructural correlations, the folded μ_3-phenoxido/μ_3-hydroxido/μ-*syn*−*anti*-carboxylate triple-bridged fragments in complex **1**, described by the exchange coupling J_1 and possessing mean θ and τ angles of 90.7° and 52.0° and a β of 27.4°, should transmit F interactions between the Ni^{II} ions. This conclusion is in agreement with the ferromagnetic interaction experimentally found for this magnetic pathway. Moreover, the weak antiferromagnetic interaction found for the double μ_3-phenoxido/μ_3-hydroxido bridges present in the cubane structure of **1** is not unexpected because they have θ angles of approximately 100° and almost planar $Ni(O)_2Ni$ bridging fragments.

The tetranuclear Ni_4 complex **2** has three different magnetic exchange pathways between Ni^{II} ions: (i) a μ-phenoxido/*syn*−*syn*-acetate/μ_3-methoxido mixed triple bridge, (ii) a μ_3-methoxido/$\mu_{1,1}$-azide double bridge, and (iii) a double-μ_3-methoxido bridge, which are described by the magnetic exchange parameters J_1, J_2, and J_3, respectively. The magnetic exchange pathway (i) has a mean Ni−O−Ni angle of 93.3°, which, together with the countercomplementary effect of the acetate group, should transmit a moderate ferromagnetic interaction. Pathway ii shows mean $Ni-N_{azide}-Ni$ and $Ni-O-Ni$ angles of 97.71° and 102.26°, respectively. It has been recently shown by DFT calculations that the phenoxido and $\mu_{1,1}$-azide bridges have countercomplementary effects on the magnetic exchange coupling, so that the ferromagnetic interaction increases with increasing $Ni-N_{azide}-N/Ni-N_{azide}$ ratio and decreases with decreasing $Ni-O_{phenoxido}-Ni/Ni-O_{phenoxido}$ ratio.[60] Assuming the same behavior for the μ_3-methoxido/$\mu_{1,1}$-azide double mixed bridge, a ferromagnetic interaction is expected through this pathway that would be weaker than that occurring through the μ-phenoxido/*syn*−*syn*-acetate/μ_3-methoxido exchange pathway. Finally, for the double-μ_3-methoxido pathway with a mean Ni−O−Ni angle of 97.7°, a weak ferro- or antiferromagnetic interaction is expected. The observed J values for the magnetic exchange

DOI: 10.1021/acs.inorgchem.5b00039
Inorg. Chem. 2015, 54, 4709−4723

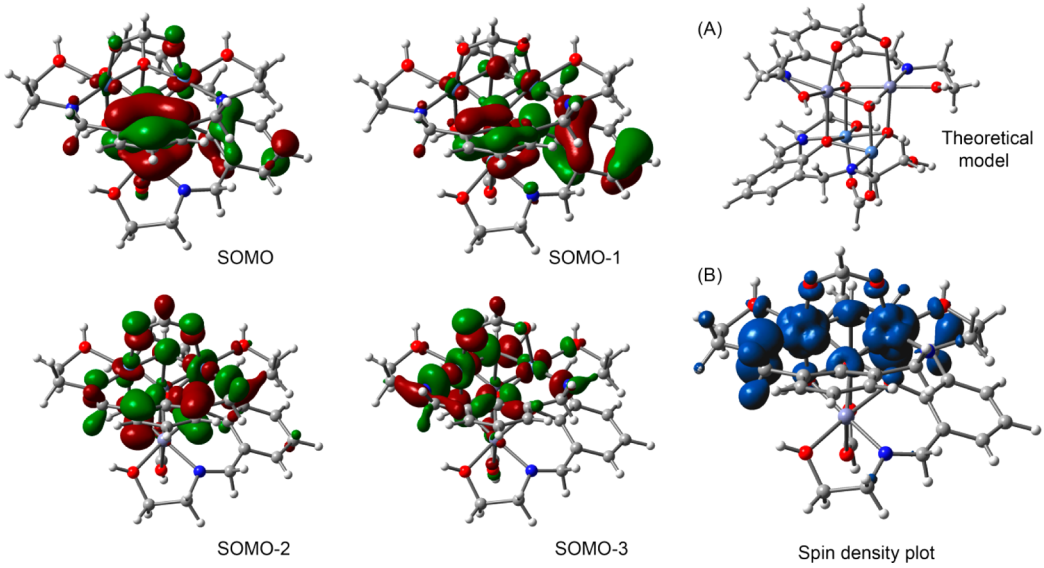

Figure 8. Pictorial representation of the SOMO involving the $d_{x^2-y^2}$ and d_{z^2} orbitals of Ni^{II} of compound **1**. (A) Theoretical model used for the calculations. (B) Graphical representation of the spin density (contour 0.004 e $Å^{-3}$) at the ground-state (high-spin) configuration of compound **1**.

pathways i–iii agree well with the above predictions and with experimental results for analogous cubane complexes.[61] The magnetic exchange constants for other Ni^{II}-based defective dicubanes found in the literature are summarized in Table 3.

In **3**, the μ-phenoxo/μ-single carbonato bridges connecting the Ni1/Ni2, Ni5/Ni6, and Ni3/Ni4 pairs have θ angles of approximately 100°, and therefore the weak antiferromagnetic interactions observed for these exchange pathways (described as J_1 and J_2) are not unexpected. The μ-dialkoxo pathways connecting the Ni2/Ni3 and Ni4/Ni5 pairs show small θ and large τ angles with mean values of 89.5° and 60.1°, respectively. Therefore, a ferromagnetic interaction is expected for this exchange pathway, which agrees well with the experimentally found J_3 value. The magnetic exchange constants for other carbonate-bridged nickel(II) complexes found in the literature are summarized in Table 4.

Spin-Density Distribution Analysis for Possible Magnetic Interactions in 1–3. In order to provide the magnetic coupling interactions theoretically, the spin-density distribution is analyzed in compounds **1**–**3**. According to the molecular orbital theory, spin delocalization is the result of electron transfer from the magnetic centers to the ligand atoms. For compound **1**, a spin-exchange model was generated for theoretical studies using the crystal structure geometry. The theoretical model has been simplified, i.e., H atoms instead of methyl/*tert*-butyl groups have been used in order to keep the size of the system computationally approachable (see Figure 8A).

Calculation of the individual pairwise exchange constants has been performed by changing two Ni atoms by two Zn atoms. This procedure not only saves computational time but also was found to give accurate results (close to the experimentally fitted values) compared to the tetranuclear models.[62] Spin-unrestricted DFT calculations were performed on the model dimer [Ni_2] complex that presents the highest experimental J value (+11.4 cm^{-1}) using the B3LYP method and employing the 6-31+G* basis set. The other two J values are very small (~2 cm^{-1}), and we have not performed theoretical calculations using their corresponding model dimers because they fall within the accuracy of the theoretical method and intrinsic experimental error. Therefore, we have only examined the magnetic coupling mechanism of $J_{Ni1-Ni3} = J_{Ni2-Ni4}$, analyzing the singly occupied molecular orbitals (SOMOs) and spin-density distribution. The theoretical J value is 13.4 cm^{-1}, which is in good agreement with the experimental value (11.4 cm^{-1}) and confirms the ferromagnetic coupling between both metal centers (see Table 5). Mulliken spin population analysis (see Table S4 in the SI) indicates that a significant spin (ca. 0.45 e) is delocalized through the ligands, and the rest (3.55 e) is carried by the Ni atoms. The spin-density plot is shown in Figure 8B for the high-spin state of **1**. The spin-density distribution shows a delocalization mechanism in which the Ni atoms carry 84.5% of the net spin and the remaining part is delocalized through coordinating atoms. The spin density is slightly higher in the phenoxido (0.10 e) O atom compared to the μ_3-OH (0.07 e) O atom, which indicates that bridging phenoxido O atoms are more effective for mediating magnetic exchange. The spin density is even smaller in the carboxylate-bridged (0.05 and 0.06 e) O atoms.

Table 5. Experimental and Theoretical Magnetic Coupling Constants J (cm^{-1}) Obtained for Complexes 1–3

	J_1		J_2		J_3	
compound	exp	theor	exp	theor	exp	theor
1	+11.4	+13.4	+2.1	n.a.	−2.8	n.a.
2	+27.5	+12.4	+20.6	+19.6	+1.52	n.a.
3	−3.3	−6.6	+1.7	n.a.	−12.8	−22.5

In octahedral nickel(II) complexes, each orbital ($d_{x^2-y^2}$ and d_{z^2}) contains an unpaired electron; consequently, these orbitals, along with the local orbitals of the bridging ligands, are involved in the superexchange pathway. This behavior is also observed in the orbital analysis of complex **1**. The SOMOs involving the d_{z^2} and $d_{x^2-y^2}$ (see SOMO to SOMO−3 in Figure 8) atomic orbitals of Ni^{II} metal centers are represented in Figure 8, where the participation of the p orbitals of the O atoms of phenoxide and the μ_3-OH bridge can also be observed. The contributions of the d_{z^2} and $d_{x^2-y^2}$ orbitals are 21, 19, 23, and 22% for SOMO, SOMO−1, SOMO−2, and SOMO−3, respectively.

DOI: 10.1021/acs.inorgchem.5b00039
Inorg. Chem. 2015, 54, 4709–4723

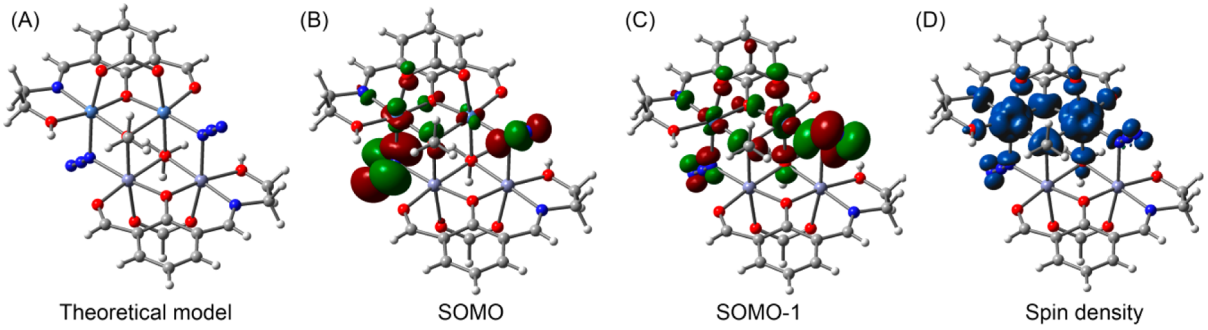

Figure 9. (A) Theoretical model used for the calculations. (B and C) Pictorial representation of the SOMO involving the $d_{x^2-y^2}$ and d_{z^2} orbitals of Ni^{II} of compound **2**. (D) Spin-density plot (contour 0.004 e $Å^{-3}$) of the high-spin configuration of compound **2**.

Similar to **1**, compound **2** presents a ferromagnetic exchange coupling inside its tetranickel dicubane unit. The spin-exchange models were generated for theoretical studies using the crystal structure geometry (see Figure 9A), and they have been simplified (H atoms instead of methyl groups apart from the methyl of the μ_3-OMe ligand, which has been conserved) in order to keep the size of the system computationally approachable. The tetranuclear complex was split into two $[Ni_2]$ dimer model complexes to calculate the individual pairwise exchange constants by using the whole structure and changing the corresponding Ni atoms by two Zn atoms. We have not performed the DFT study for J_3 because it is very small (1.52 cm^{-1}). The calculated values for the other two are J_1 = 12.4 cm^{-1} and J_2 = 19.6 cm^{-1}, which confirm the ferromagnetic couplings. The value of J_2 is in very good agreement with the experimental value; however, J_1 is slightly underestimated by the theoretical method (see Table 5). In order to further examine the magnetic coupling mechanism, the spin-density distribution has been analyzed. For the $[Ni_2]$ dimer that corresponds to the J_1 coupling, Mulliken spin population analysis indicates that a significant spin (ca. 0.60 e) is delocalized through the ligands, and the rest (3.40 e) is carried by the central Ni atoms. The spin-density plot is shown in Figure 9 for the high-spin state of **2**. The spin density (see Table S5 in the SI) is much lower in the phenoxido (0.07 e) O atom compared to the μ_3-OCH_3 (0.13 e) O atom, which indicates that the μ_3-OCH_3 bridging is more effective for mediating magnetic exchange. For the $[Ni_2]$ dimer that corresponds to the J_2 coupling, Mulliken spin population analysis also indicates that a significant spin (ca. 0.53 e) is delocalized through the ligands, and the rest (3.47 e) is carried by the central Ni atoms. In contrast to the J_1 coupling mechanism, the spin density (see Table S5 in the SI) is much lower in the μ_3-OCH_3 (0.09 e) O atom compared to the azide (0.13 e), which indicates that the azide bridging is more effective for mediating magnetic exchange.

The SOMOs involving the d_{z^2} and $d_{x^2-y^2}$ (SOMO and SOMO−1) orbitals of Ni^{II} metal centers are represented in Figure 9 for the model dimer that corresponds to J_1, where the participation of the p orbitals of the bridging O atoms of phenoxide and the μ_3-OCH_3 ligand can be clearly observed. This analysis confirms that both $d_{x^2-y^2}$ and d_{z^2} orbitals of Ni^{II} and ligand local orbitals are responsible of the superexchange phenomena. The orbital and spin-density plots are similar for the other model dimer (J_2), where the p orbitals of the azide ligand are involved in the superexchange pathway instead of the phenoxide.

As indicated above, compound **3** exhibits two antiferromagnetic couplings (J_1 and J_3) and one weak ferromagnetic exchange coupling (J_2) inside its hexanickel core. Two spin-exchange models were generated for theoretical studies using the crystal structure geometry (see Figure 10), and they have been simplified (H atoms instead of methyl groups in the L ligand) in order to keep the size of the system computationally approachable. The hexanuclear complex was split into two $[Ni_2]$ dimer model complexes to calculate the individual antiferromagnetic pairwise exchange constants by using the whole structure and changing four Ni atoms by Zn atoms. The calculated J values are J_1 = −6.6 cm^{-1} and J_3 = −22.5 cm^{-1}, which are in reasonable agreement with the experiment (J_1 = −3.3 cm^{-1} and J_3 = −12.8 cm^{-1}, which confirms the antiferromagnetic coupling; see Table 5). In order to further examine the magnetic coupling mechanism, the spin-density distribution has been analyzed. For the $[Ni_2]$ dimer that corresponds to the J_1 coupling, Mulliken spin population analysis indicates that a significant spin (ca. 0.62 e) is delocalized through the ligands, and the rest (3.38 e) is carried by the central Ni atoms. The spin-density plot is shown in Figure 10 for the high-spin state of **3**. The spin density (see

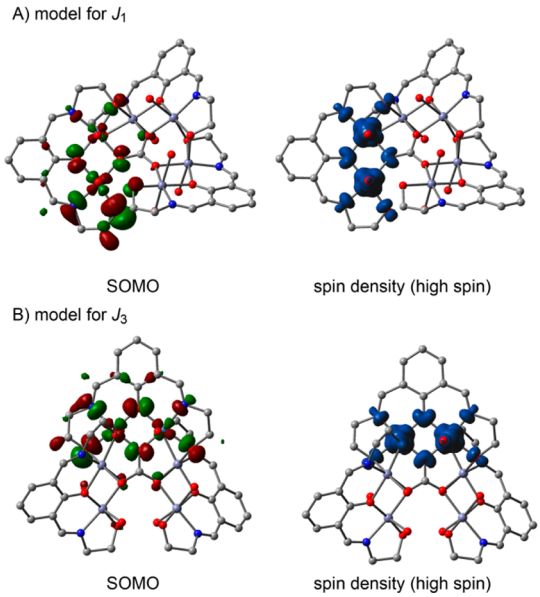

Figure 10. Pictorial representation of the SOMO involving the $d_{x^2-y^2}$ and d_{z^2} orbitals of Ni^{II} of compound **3**. Right: spin-density plot of the high-spin configuration of compound **3**.

DOI: 10.1021/acs.inorgchem.5b00039
Inorg. Chem. 2015, 54, 4709−4723

Table S6 in the SI) is similar in both the phenoxido and carboxylate O atoms (~0.07 e), which indicates that both bridging atoms are equally effective for mediating magnetic exchange. The spin carried by both atoms is negligible in the broken-symmetry state of complex **3**, indicating a polarization competition between the two Ni atoms with α and β spin density, respectively.

For the [Ni_2] dimer that corresponds to the J_3 coupling, Mulliken spin population analysis also indicates that a significant spin (ca. 0.71 e) is delocalized through the ligands, and the rest (3.29 e) is carried by the central Ni atoms. The spin delocalization is higher in this dimer (Ni3−Ni4 coupling), in agreement with its larger J value. In this case, the spin density (see Table S6 in the SI) is slightly lower in the phenoxido (0.08 e) O atom compared to the carbonato (0.09 e) O atom.

In compound **3**, only the $d_{x^2-y^2}$ orbitals of the metal atom along with the local orbitals of the bridging ligands are involved in the superexchange pathways. The SOMOs involving the $d_{x^2-y^2}$ orbitals of Ni^{II} metal centers are represented in Figure 10, where the participation of the p orbitals of the bridging O atoms of phenoxide and the μ_6-CO_3 ligand can be clearly observed.

CONCLUSIONS

Complexation of the phenolate-centered multidentate ligand 2,6-bis[(2-hydroxy-(1,1-dimethylethyl)imino]methyl]-4-methylphenol with nickel(II) nitrate and perchlorate led to three types of self-assembled supradinuclear aggregates. Isolation of two tetranuclear [Ni_4] and one hexanuclear [Ni_6] clusters followed from in situ generated and trapped HO^-, MeO^-, and CO_3^{2-} ions from water, MeOH, and atmospheric CO_2. These three anions have been used to control the molecular topology of the final products. The ligand H_3L in its different forms is initially able to trap two Ni^{II} ions, leaving behind available coordinating sites for coordination of hydroxido, methoxido, azido, and carbonato anios, which facilitate the assembly of two or three ligand-bound Ni^{II} pairs. The composition of these homometallic clusters was supported by X-ray crystallography, elemental analysis, and magnetic susceptibility measurements.. Complexes **1** and **3** exhibit intramolecular antiferro- and ferromagnetic interactions between the Ni^{II} ions, whereas in compound **2**, all of the magnetic exchange pathways transmit ferromagnetic interactions, leading to a S = 4 ground state. Complexes **1** and **3** show in the low-temperature region a magnetic behavior that could be related either to spin glass or to the existence of a trace amount of an extended metal complex or a disordered structure with nonnegligible intercluster interactions.

Analysis of the experimental and DFT-calculated sign and magnitude of the coupling constants gives a complete description of the magnetic properties of this kind of self-assembled multimetallic system. The bridging atoms and atomic orbitals of ligands and metal centers involved in the superexchange pathways have been studied by the spin-density and SOMO plots. We are currently working on other ancillary bridges such as sulfido, nitrito, nitrato, thiocyanato, cyanato, oximato, etc., in this reaction system to induce the formation of new types of homo- and heterometallic self-assembled cage complexes of higher nuclearity.

ASSOCIATED CONTENT

Supporting Information

X-ray crystallographic data in CIF format, Schemes S1−S5, Figures S1−S16, Tables S1−S6, and synthesis and characterization of ligand H_3L. The Supporting Information is available free of charge on the ACS Publications website at DOI: 10.1021/acs.inorgchem.5b00039.

AUTHOR INFORMATION

Corresponding Author

*E-mail: dray@chem.iitkgp.ernet.in. Tel: (+91) 3222-283324. Fax: (+91) 3222-82252.

Notes

The authors declare no competing financial interest.

ACKNOWLEDGMENTS

M.P. is thankful to the Council of Scientific and Industrial Research, New Delhi, India, for financial support. The authors also give thanks to DST, New Delhi, India, for providing the Single Crystal X-ray Diffractometer facility in the Department of Chemistry, IIT Kharagpur, under its FIST program. E.C. is thankful for financial support from the Spanish Ministerio de Economía y Competitividad (Project CTQ 2011-24478 and CTQ-2014-56312-P), the Junta de Andalucía (FQM-195, the Project of excellence P11-FQM-7756), and the University of Granada. A.B. and A.F. acknowledge MINECO (Projects and CONSOLIDER INGENIO 2010, CSD2010-00065, and FEDER funds) and the Direcció General de Recerca i Innovació del Govern Balear (Project 23/2011 and FEDER funds) for financial support. We thank the CTI (UIB) for free allocation of computer time.

REFERENCES

(1) Kostakis, G. E.; Ako, A. M.; Powell, A. K. *Chem. Soc. Rev.* **2010**, *39*, 2238−2271.

(2) Ribas, J.; Escuer, A.; Monfort, M.; Vicente, R.; Cortés, R.; Lezama, L.; Rojo, T. *Coord. Chem. Rev.* **1999**, *193*, 1027−1068.

(3) (a) Christou, G.; Gatteschi, D.; Hendrickson, D. N.; Sessoli, R. *MRS Bull.* **2000**, 66−71. (b) Krzystek, J.; Telser, J.; Pardi, L. A.; Goldberg, D. P.; Hoffman, B. M.; Brunel, L.-C. *Inorg. Chem.* **1999**, *38*, 6121−6129.

(4) (a) Sarkar, M.; Aromí, G.; Cano, J.; Bertolasi, V.; Ray, D. *Chem.—Eur. J.* **2010**, *16*, 13825−13833. (b) Ghosh, A. K.; Pait, M.; Clérac, R.; Mathonière, C.; Bertolasi, V.; Bauzá, A.; Frontera, A.; Pramanik, K.; Ray, D. *Dalton Trans.* **2014**, *43*, 4076−4085. (c) Ghosh, A. K.; Pait, M.; Shatruk, M.; Bertolasi, V.; Ray, D. *Dalton Trans.* **2014**, *43*, 1970−1973.

(5) (a) Jia, H.-P.; Zhan-Feng Ju, W. L.; Zhang, J. *Chem. Commun.* **2008**, 371−373. (b) Palli, A. V.; Reu, O. S.; Ostrovsky, S. M.; Klokishner, S. I.; Tsukerblat, B. S.; Sun, Z.-M.; Mao, J.-G.; Prosvirin, A. V.; Zhao, H.-H.; Dunbar, K. R. *J. Am. Chem. Soc.* **2008**, *130*, 14729−14738. (c) Li, J.-R.; Yu, Q.; Tao, Y.; Bu, X.-H.; Ribas, J.; Batten, S. R. *Chem. Commun.* **2007**, 2290−2292. (d) Cao, D.-K.; Li, Y.-Z.; Zheng, L. M. *Inorg. Chem.* **2007**, *46*, 7571−7578.

(6) (a) Sourlas, N. *Nature* **1989**, *339*, 693−695. (b) Taniguchi, T.; Yamanaka, K.; Sumioka, H.; Yamazaki, T.; Tabata, Y.; Kawarazaki, S. *Phys. Rev. Lett.* **2004**, *93*, 246605. (c) Liu, X.-T.; Wang, X.-Y.; Zhang, W.-X.; Cui, P.; Gao, S. *Adv. Mater.* **2006**, *18*, 2852−2856.

(7) (a) Figuerola, A.; Tangoulis, V.; Ribas, J.; Hartl, H.; Brudgam, I.; Maestro, M.; Diaz, C. *Inorg. Chem.* **2007**, *46*, 11017−11024. (b) Prinz, M.; Kuepper, K.; Taubitz, C.; Raekers, M.; Khanra, S.; Biswas, B.; Weyhermüller, T.; Uhlarz, M.; Wosnitza, J.; Schnack, J.; Postnikov, A. V.; Schrüder, C.; George, S. J.; Neumann, M.; Chaudhuri, P. *Inorg. Chem.* **2010**, *49*, 2093−2102.

DOI: 10.1021/acs.inorgchem.5b00039
Inorg. Chem. 2015, 54, 4709−4723

(8) (a) Chen, S.-Y.; Beedle, C. C.; Gan, P.-R.; Lee, G.-H.; Hill, S.; Yang, E.-C. *Inorg. Chem.* **2012**, *51*, 4448−4457. (b) Caneschi, A.; Gatteschi, D.; Sessoli, R.; Barra, A. L.; Brunel, L. C.; Guillot, M. *J. Am. Chem. Soc.* **1991**, *113*, 5873−5874. (c) Aubin, S. M. J.; Dilley, N. R.; Pardi, L.; Krzystek, J.; Wemple, M. W.; Brunel, L.-C.; Maple, M. B.; Christou, G.; Hendrickson, D. N. *J. Am. Chem. Soc.* **1998**, *120*, 4991−5004. (d) Gatteschi, D.; Sessoli, R. *Angew. Chem., Int. Ed.* **2003**, *42*, 268−297. (e) Oshio, H.; Nakano, M. *Chem.—Eur. J.* **2005**, *11*, 5178−5185. (f) Bircher, R.; Chaboussant, G.; Dobe, C.; Gudel, H. U.; Ochsenbein, S. T.; Sieber, A.; Waldmann, O. *Adv. Funct. Mater.* **2006**, *16*, 209−220. (g) Aromí, G.; Brechin, E. K. *Struct. Bonding (Berlin)* **2006**, *122*, 1−67. (h) Powell, A. K. *Nat. Chem.* **2010**, *2*, 351−352.

(9) Rey, N. A.; Neves, A.; Bortoluzzi, A. J.; Pich, C. T.; Terenzi, H. *Inorg. Chem.* **2007**, *46*, 348−350.

(10) (a) Sarkar, M.; Clérac, R.; Mathonière, C.; Hearns, N. G. R.; Bertolasi, V.; Ray, D. *Inorg. Chem.* **2010**, *49*, 6575−6585. (b) Sarkar, M.; Clérac, R.; Mathonière, C.; Hearns, N. G. R.; Bertolasi, V.; Ray, D. *Inorg. Chem.* **2011**, *50*, 3922−3933.

(11) Ghosh, A. K.; Shatruk, M.; Bertolasi, V.; Pramanik, K.; Ray, D. *Inorg. Chem.* **2013**, *52*, 13894−13903.

(12) (a) Halcrow, M. A.; Sun, J.-S.; Huffman, J. C.; Christou, G. *Inorg. Chem.* **1995**, *34*, 4167−4177. (b) Mandal, D.; Hong, C. S.; Kim, H. C.; Fun, H.-K.; Ray, D. *Polyhedron* **2008**, *27*, 2372−2378. (c) Sieber, A.; Boskovic, C.; Bircher, R.; Waldmann, O.; Ochsenbein, S. T.; Chaboussant, G.; Güdel, H. U.; Kirchner, N.; Slageren, J. v.; Wernsdorfer, W.; Neels, A.; Stoeckli-Evans, H.; Janssen, S.; Juranyi, F.; Mutka, H. *Inorg. Chem.* **2005**, *44*, 4315−4325. (d) Meally, S. T.; Taylor, S. M.; Brechin, E. K.; Piligkos, S.; Jones, L. F. *Dalton Trans.* **2013**, *42*, 10315−10325. (e) Zhang, S.-Y.; Chen, W.-Q.; Hu, B.; Chen, Y.-M.; Li, W.; Li, Y. *Inorg. Chem. Commun.* **2012**, *16*, 74−77. (f) Hudson, T. A.; Berry, K. J.; Moubaraki, B.; Murray, K. S.; Robson, R. *Inorg. Chem.* **2006**, *45*, 3549−3556. (g) Ferguson, A.; Schmidtmann, M.; Brechin, E. K.; Murrie, M. *Dalton Trans.* **2011**, 334−336. (h) Karmakar, S.; Khanra, S. *CrystEngComm* **2014**, *16*, 2371−2383. (i) Das, A.; Klinke, F. J.; Demeshko, S.; Meyer, S.; Dechert, S.; Meyer, F. *Inorg. Chem.* **2012**, *51*, 8141−8149. (j) Ponomaryov, A. N.; Kim, N.; Hwang, J.; Nojiri, H.; Tol, J. v.; Ozarowski, A.; Park, J.; Jang, Z.; Suh, B.; Yoon, S.; Choi, K.-Y. *Chem.—Asian J.* **2013**, *8*, 1152−1159. (k) Liang, Q.; Huang, R.; Chen, X.; Li, Z.; Zhang, X.; Sun, B. *Inorg. Chem. Commun.* **2010**, *13*, 1134−1136.

(13) (a) Serna, Z. E.; Lezama, L.; Urtiaga, M. K.; Arriortua, M. I.; Barandika, M. G.; Cortés, R.; Rojo, T. *Angew. Chem., Int. Ed.* **2000**, *39*, 344−347. (b) Serna, Z.; Pinta, N. D. l.; Urtiaga, M. K.; Lezama, L.; Madariaga, G.; Clemente-Juan, J. M.; Coronado, E.; Cortés, R. *Inorg. Chem.* **2010**, *49*, 11541−11549. (c) Banerjee, S.; Nandy, M.; Sen, S.; Mandal, S.; Rosair, G. M.; Slawin, A. M. Z.; Gómez García, C. J.; Clemente-Juan, J. M.; Zangrando, E.; Guidoling, N.; Mitra, S. *Dalton Trans.* **2011**, *40*, 1652−1661. (d) Clemente-Juan, J. M.; Coronado, E.; Galán-Mascarós, J. R.; Gómez-García, C. J. *Inorg. Chem.* **1999**, *38*, 55−63. (e) Serna, Z. E.; Barandika, M. G.; Cortées, R.; Urtiaga, M. K.; Barberis, G. E.; Rojo, T. *J. Chem. Soc., Dalton Trans.* **2000**, 29−34. (f) Wu, D.-Y.; Huang, W.; Hua, W.-H.; Song, Y.; Duan, C.-Y.; Li, S.-H.; Meng, Q.-J. *Dalton Trans.* **2007**, 1838−1845.

(14) Esteban, J.; Ruiz, E.; Font-Bardia, M.; Calvet, T.; Escuer, A. *Chem.—Eur. J.* **2012**, *18*, 3637−3648.

(15) (a) Biswas, R.; Ida, Y.; Baker, M. L.; Biswas, S.; Kar, P.; Nojiri, H.; Ishida, T.; Ghosh, A. *Chem.—Eur. J.* **2013**, *19*, 3943−3953. (b) Hazra, S.; Koner, R.; Lemoine, P.; Sañudo, E. C.; Mohanta, S. *Eur. J. Inorg. Chem.* **2009**, 3458−3466. (c) Mandal, D.; Bertolasi, V.; Ribas-Ariño, J.; Aromí, G.; Ray, D. *Inorg. Chem.* **2008**, *47*, 3465−3467.

(16) (a) Massoud, S. S.; Mautner, F. A.; Vicente, R.; Gallo, A. A.; Ducasse, E. *Eur. J. Inorg. Chem.* **2007**, 1091−1102. (b) Goher, M. A. S.; Escuer, A.; Mautner, F. A.; Al-Salem, N. A. *Polyhedron* **2002**, *21*, 1871−1876.

(17) (a) Cortes, R.; Pizarro, J. L.; Lezama, L.; Arriortua, M. I.; Rojo, T. *Inorg. Chem.* **1994**, *33*, 2697−2700. (b) Karmakar, T. K.; Chandra, S. K.; Ribas, J.; Mostafa, G.; Luc, T. H.; Ghosh, B. K. *Chem. Commun.* **2002**, 2364−2365. (c) Sarkar, S.; Mondal, A.; Fallah, M. S. E.; Ribas, J.; Chopra, D.; Stoeckli-Evans, H.; Rajak, K. K. *Polyhedron* **2006**, *25*, 25−30. (d) Biswas, R.; Mukherjee, S.; Kar, P.; Ghosh, A. *Inorg. Chem.* **2012**, *51*, 8150−8160.

(18) Weinstock, I. A. *Chem. Rev.* **1998**, *98*, 113−170.

(19) (a) Scheurer, A.; Gieb, K.; Alam, M. S.; Heinemann, F. W.; Saalfrank, R. W.; Kroener, W.; Petukhov, K.; Stockerb, M.; Müller, P. *Dalton Trans.* **2012**, *41*, 3553−3561. (b) Petit, S.; Neugebauer, P.; Pilet, G.; Chastanet, G.; Barra, A.-L.; Antunes, A. B.; Wernsdorfer, W.; Luneau, D. *Inorg. Chem.* **2012**, *51*, 6645−6654. (c) Stamatatos, T. C.; Escuer, A.; Abboud, K. L.; Raptopoulou, C. P.; Perlepes, S. P.; Christou, G. *Inorg. Chem.* **2008**, *47*, 11825−11838. (d) Escuer, A.; Esteban, J.; Nuria, A.-A.; Font-Bardia, M.; Calvet, T.; Roubeau, O.; Teat, S. J. *Inorg. Chem.* **2010**, *50*, 2259−2266.

(20) (a) Mukherjee, S.; Weyhermüller, T.; Bothe, E.; Wieghardt, K.; Chaudhuri, P. *Eur. J. Inorg. Chem.* **2003**, 863−875. (b) Papatriantafyllopoulou, C.; Stamatatos, T. C.; Wernsdorfer, W.; Teat, S. J.; Tasiopoulos, A. J.; Escuer, A.; Perlepes, S. P. *Inorg. Chem.* **2010**, *49*, 10486−10496. (c) Escuer, A.; Vlahopouloua, G.; Mautnerb, F. A. *Dalton Trans.* **2011**, *40*, 10109−10116. (d) Pons-Balague, A.; Ioanidis, N.; Wernsdorfer, W.; Yamaguchi, A.; Sanudo, E. C. *Dalton Trans.* **2011**, *40*, 11765−11769.

(21) (a) Ray, M. S.; Ghosh, A.; Das, A.; Drew, M. G. B.; Ribas-Ariño, J.; Novoa, J.; Ribas, J. *Chem. Commun.* **2004**, 1102−1103. (b) Wang, Z.; Zhang, B.; Kurmoo, M.; Green, M. A.; Fujiwara, H.; Otsuka, T.; Kobayashi, H. *Inorg. Chem.* **2005**, *44*, 1230−1237. (c) Wang, Z.; Zhang, B.; Inoue, K.; Fujiwara, H.; Otsuka, T.; Kobayashi, H.; Kurmoo, M. *Inorg. Chem.* **2007**, *46*, 437−445. (d) Liu, T.; Zhang, Y.; Yang, Z.; Gao, S. *Inorg. Chem.* **2006**, *45*, 2782−2784.

(22) Mikuriya, M.; Murase, I.; Asato, E.; Kida, S. *Chem. Lett.* **1989**, 497−500.

(23) Rawle, S. C.; Harding, C. J.; Moore, P.; Alcock, N. W. *J. Chem. Soc., Chem. Commun.* **1992**, 1701−1703.

(24) Kempe, R.; Sieler, J.; Walther, D.; Reinhold, J.; Rommel, K. *Z. Anorg. Allg. Chem.* **1993**, *619*, 1105−1110.

(25) Yamada, K.; Hori, K.; Fukuda, Y. *Acta Crystallogr., Sect. C* **1993**, *49*, 445−448.

(26) Kitajima, N.; Hikichi, S.; Tanaka, M.; Moro-oka, Y. *J. Am. Chem. Soc.* **1993**, *115*, 5496−5508.

(27) Lozano, A. A.; Sáez, M.; Pérez, J.; García, L.; Lezama, L.; Rojo, T.; López, G.; Garcíaa, G.; Santana, M. D. *Dalton Trans.* **2006**, 3906−3911.

(28) Escuer, A.; Vicente, R.; Kumar, S. B.; Solans, X.; Font-Bardia, M.; Caneschi, A. *Inorg. Chem.* **1996**, *35*, 3094−3098.

(29) Mukherjee, P.; Drew, M. G. B.; Estrader, M.; Ghosh, A. *Inorg. Chem.* **2008**, *47*, 7784−7791.

(30) Georgopoulou, A. N.; Raptopoulou, C. P.; Psycharis, V.; Ballesteros, R.; Abarca, B.; Boudalis, A. K. *Inorg. Chem.* **2009**, *48*, 3167−3176.

(31) Tong, M.-L.; Monfort, M.; Juan, J. M. C.; Chen, X.-M.; Bu, X.-H.; Ohbad, M.; Kitagawa, S. *Chem. Commun.* **2005**, 233−235.

(32) Cooper, G. J. T.; Newton, G. N.; Kögerler, P.; Long, D.-L.; Engelhardt, L.; Luban, M.; Cronin, L. *Angew. Chem., Int. Ed.* **2007**, *46*, 1340−1344.

(33) Dhara, K.; Saha, U. C.; Dan, A.; Sarkar, S.; Manassero, M.; Chattopadhyay, P. *Chem. Commun.* **2010**, 1754−1756.

(34) (a) Noodleman, L. *J. Chem. Phys.* **1981**, *74*, 5737−5743. (b) Noodleman, L.; Davidson, E. R. *Chem. Phys.* **1986**, *109*, 131−143.

(35) Noodleman, L.; Peng, C. Y.; Case, D. A.; Mouesca, J. M. *Coord. Chem. Rev.* **1995**, *144*, 199−244.

(36) Frisch, M. J.; Trucks, G. W.; Schlegel, H. B.; Scuseria, G. E.; Robb, M. A.; Cheeseman, J. R.; Scalmani, G.; Barone, V.; Mennucci, B.; Petersson, G. A.; Nakatsuji, H.; Caricato, M.; Li, X.; Hratchian, H. P.; Izmaylov, A. F.; Bloino, J.; Zheng, G.; Sonnenberg, J. L.; Hada, M.; Ehara, M.; Toyota, K.; Fukuda, R.; Hasegawa, J.; Ishida, M.; Nakajima, T.; Honda, Y.; Kitao, O.; Nakai, H.; Vreven, T.; Montgomery, J. A., Jr.; Peralta, J. E.; Ogliaro, F.; Bearpark, M.; Heyd, J. J.; Brothers, E.; Kudin, K. N.; Staroverov, V. N.; Kobayashi, R.; Normand, J.; Raghavachari, K.; Rendell, A.; Burant, J. C.; Iyengar, S. S.; Tomasi, J.; Cossi, M.; Rega, N.; Millam, M. J.; Klene, M.; Knox, J. E.; Cross, J. B.; Bakken, V.;

DOI: 10.1021/acs.inorgchem.5b00039
Inorg. Chem. 2015, 54, 4709−4723

Adamo, C.; Jaramillo, J.; Gomperts, R.; Stratmann, R. E.; Yazyev, O.; Austin, A. J.; Cammi, R.; Pomelli, C.; Ochterski, J. W.; Martin, R. L.; Morokuma, K.; Zakrzewski, V. G.; Voth, G. A.; Salvador, P.; Dannenberg, J. J.; Dapprich, S.; Daniels, A. D.; Farkas, Ö.; Foresman, J. B.; Ortiz, J. V.; Cioslowski, J.; Fox, D. J. *Guassian 09*; Gaussian, Inc.: Wallingford, CT, 2009.
(37) Onofrio, N.; Mouesca, J.-M. *Inorg. Chem.* **2011**, *50*, 5577−5586.
(38) (a) Neese, F. *Coord. Chem. Rev.* **2009**, *253*, 526−563. (b) Neese, F.; Petrenko, T.; Ganyushin, D.; Olbrich, G. *Coord. Chem. Rev.* **2007**, *251*, 288−327.
(39) (a) Adamo, C.; Barone, V.; Bencini, A.; Broer, R.; Filatov, M.; Harrison, N. M.; Illas, F.; Malrieuand, J. P. *J. Chem. Phys.* **2006**, *124*, 107101. (b) Adamo, C.; Barone, V. *J. Chem. Phys.* **1999**, *110*, 6158. (c) Adamo, C.; di Matteo, A.; Barone, V. *Adv. Quantum Chem.* **2000**, *36*, 45.
(40) Miralles, J.; Castell, O.; Caballol, R.; Malrieu, J. P. *Chem. Phys.* **1993**, *33*, 172.
(41) *SAINT, SMART, and XPREP*; Siemens Analytical X-ray Instruments Inc.: Madison, WI, 1995.
(42) (a) Sheldrick, G. M. *SHELXS-97*; University of Göttingen: Göttingen, Germany, 1997. (b) Sheldrick, G. M. *SHELXL 97, Program for Crystal Structure Refinement*; University of Göttingen: Göttingen, Germany, 1997.
(43) Sheldrick, G. M. *SADABS: Software for Empirical Absorption Correction*; University of Göttingen and Institute fur Anorganische Chemieder Universitat: Göttingen, Germany, 1999−2003.
(44) Ghosh, A. K.; Bauzá, A.; Bertolasi, V.; Frontera, A.; Ray, D. *Polyhedron* **2013**, *5*, 32−39.
(45) Sarkar, A.; Ghosh, A. K.; Bertolasi, V.; Ray, D. *Dalton Trans.* **2012**, *41*, 1889−1896.
(46) Deacon, G. B.; Phillips, R. J. *Coord. Chem. Rev.* **1980**, *33*, 227−250.
(47) Nakamoto, K. *Infrared and Raman Spectra of Inorganic and Coordination Compounds*, 4th ed.; Wiley: New York, 1986.
(48) Demeshko, S.; Leibeling, G.; Maringgele, W.; Meyer, F.; Mennerich, C.; Klauss, H. H.; Pritzkow, H. *Inorg. Chem.* **2005**, *44*, 519−528.
(49) (a) Liang, X.; Parkinson, J. A.; Parsons, S.; Weishaupl, M.; Sadler, P. J. *Inorg. Chem.* **2002**, *41*, 4539−4547. (b) Langley, S. K.; Moubaraki, B.; Murray, K. S. *Inorg. Chem.* **2012**, *51*, 3947−3949.
(50) Salawu, O. W.; Aliyu, A. O. C. *Adv. Pure Appl. Chem.* **2012**, *1*, 12−17.
(51) Paital, A. R.; Mikuriya, M.; Ray, D. *Eur. J. Inorg. Chem.* **2007**, 5360−5369.
(52) (a) Ghosh, A. K.; Bauza, A.; Bertolasi, V.; Frontera, A.; Ray, D. *Polyhedron* **2013**, *53*, 32−39. (b) Chattopadhyay, T.; Mukherjee, M.; Mondal, A.; Maiti, P.; Banerjee, A.; Banu, K. S.; Bhattacharya, S.; Roy, B.; Chattopadhyay, D. J.; Mondal, T. K. *Inorg. Chem.* **2010**, *49*, 3121−3129. (c) Biswas, A.; Das, L. K.; Drew, M. G. B.; Aromi, G.; Gamez, P.; Ghosh, A. *Inorg. Chem.* **2012**, *51*, 7993−8001.
(53) (a) Tandon, S. S.; Bunge, S. D.; Rakosi, R.; Xu, Z.; Thompson, L. K. *Dalton Trans.* **2009**, 6536−6551. (b) Tan, S.-Y.; Chang, F.; Gao, Y.-P. *Acta Crystallogr.* **2012**, *E68*, m150−m151.
(54) Mydosh, J. A. *Spin Glasses: An experimental Introduction*; Taylor and Francis: London, 1993.
(55) (a) Yang, E.-C.; Wernsdorfer, W.; Zakharov, L. N.; Karaki, Y.; Yamaguchi, A.; Isidro, R. M.; Lu, G.-D.; Wilson, S. A.; Rheingold, A. L.; Ishimoto, H.; Hendrickson, D. N. *Inorg. Chem.* **2006**, *45*, 529−546. (b) Yang, E.-C.; Wernsdorfer, W.; Hill, S.; Edwards, R. S.; Nakano, M.; Maccagnano, S.; Zakharov, L. N.; Rheingold, A. L.; Christou, G.; Hendrickson, D. N. *Polyhedron* **2003**, *22*, 1727−1733. (c) Moragues-Cánovas, M.; Helliwell, M.; Ricard, L.; Rivière, E.; Wernsdorfer, W.; Brechin, E.; Mallah, T. *Eur. J. Inorg. Chem.* **2004**, 2219−2222. (d) Ochsenbein, S. T.; Murrie, M.; Rusanow, E.; Stoeckli-Evans, H.; Sekine, C.; Udel, H.-U. G. *Inorg. Chem.* **2002**, *41*, 5133−5140. (e) Bell, A.; Aromi, G.; Teat, S. J.; Wernsdorfer, W.; Winpenny, R. E. P. *Chem. Commun.* **2005**, 2808−2810. (f) Aromí, G.; Parsons, S.; Wernsdorfer, W.; Brechin, E. K.; McInnes, E. J. L. *Chem. Commun.* **2005**, 5038−5040. (g) Ferguson, A.; Lawrence, J.; Parkin, A.; Sanchez-Benitez, J.; Kamenev, K. V.; Brechin, E. K.; Wernsdorfer, W.; Hill, S.; Murrie, M. *Dalton Trans.* **2008**, 6409−6414. (h) Lawrence, J.; Yang, E.-C.; Edwards, R.; Olmstead, M. M.; Ramsey, C.; Dalal, N. S.; Gantzel, P. K.; Hill, S.; Hendrickson, D. N. *Inorg. Chem.* **2008**, *47*, 1965−1974. (i) Hameury, S.; Kayser, L.; Pattachi, R.; Rogez, G.; Wrensdorfer, W.; Braustein, P. *Dalton Trans.* **2013**, *42*, 5013−5024. (j) Biswas, R.; Hida, Y.; Baker, M. L.; Biswas, S.; Ikar, P.; Nojiri, H.; Ishida, T.; Gosh, A. *Chem.—Eur. J.* **2013**, *19*, 3943−3953.
(56) (a) Klein, A.; Krest, A.; Nitsche, S.; Stirnat, K.; Valldor, M. *Eur. J. Inorg. Chem.* **2013**, 2757−2767. (b) Kopel, P.; Mrozinski, J.; Dolezal, K.; Langer, V.; Boca, R.; Bienko, A.; Pochaba, A. *Eur. J. Inorg. Chem.* **2009**, 5475−5482. (c) Xiong, K.; Jiang, F.; Gai, Y.; Zhou, Y.; Yuan, D.; Su, K.; Wang, X.; Hong, M. *Inorg. Chem.* **2012**, *51*, 3283−3288.
(57) Escuer, A.; Vicente, R.; Kumar, S. B.; Solans, X.; Font-Bardía, M.; Caneschi, A. *Inorg. Chem.* **1996**, *35*, 3094−3098.
(58) (a) Biswas, R.; Giri, S.; Saha, S. K.; Ghosh, A. *Eur. J. Inorg. Chem.* **2012**, 2916−1927. (b) Nanda, K. K.; Thompson, L. K.; Bridson, J. N.; Nag, K. *J. Chem. Soc., Chem. Commun.* **1994**, 1337−1338. (c) Halcrow, M. A.; Sun, J. S.; Huffman, J. C.; Christou, G. *Inorg. Chem.* **1995**, *34*, 4167−4177. (d) Clemente-Juan, J. M.; Chansou, B.; Donnadieu, B.; Tuchages, J. P. *Inorg. Chem.* **2000**, *39*, 5515−5519. (e) Bu, X. H.; Du, M.; Zhang, L.; Liao, D. Z.; Tang, J. K.; Zhang, R. H.; Shionoya, M. *J. Chem. Soc., Dalton Trans.* **2001**, 593−598. (f) Palacios, M. P.; Mota, A. J.; Perea-Buceta, J. E.; White, F. J.; Brechin, E. K.; Colacio, E. *Inorg. Chem.* **2010**, *49*, 10156−10165.
(59) Ruiz, J.; Mota, A. J.; Rodríguez-Diéguez, A.; Oyarzabal, I.; Seco, J. M.; Colacio, E. *Dalton Trans.* **2012**, *41*, 14265−14273.
(60) Sasmal, S.; Hazra, S.; Kundu, P.; Dutta, S.; Rajaraman, G.; Carolina Sañudo, E.; Mohanta, S. *Inorg. Chem.* **2011**, *50*, 7257−7267.
(61) Lin, S.-Y.; Xu, G.-F.; Zhao, L.; Guo, Y.-N.; Tang, J.; Wang, Q.-L.; Liu, G.-X. *Inorg. Chim. Acta* **2011**, *373*, 173−178.
(62) (a) Ruiz, E.; Rodríguez-Fortea, A.; Cano, J.; Alvarez, S.; Alemany, P. *J. Comput. Chem.* **2003**, *24*, 982−989. (b) Ruiz, E.; Alvarez, S.; Cano, J.; Polo, V. *J. Chem. Phys.* **2005**, *123*, 164110−164117.

DOI: 10.1021/acs.inorgchem.5b00039
Inorg. Chem. 2015, 54, 4709−4723